LITHOS 398–399 (2021) 106308

Contents lists available at ScienceDirect

LITHOS

journal homepage: www.elsevier.com/locate/lithos

Research Article

Early cretaceous crust–mantle interaction in the Middle-lower Yangtze River Metallogenic Belt, east China: Li–Nd–Sr isotopic and elemental constraints

Zhuang Li [a,b,*,1], Changjian Chen [c,**,1], Bin Chen [d], Heng'an Cai [e]

[a] State Key Laboratory of Petroleum Resources and Prospecting, China University of Petroleum (Beijing), Beijing 102249, PR China
[b] College of Geosciences, China University of Petroleum (Beijing), Beijing 102249, PR China
[c] Gemological Institute, Guilin University of Technology, Guilin 541004, PR China
[d] Department of Earth and Space Sciences, Southern University of Science and Technology, Shenzhen 518055, PR China
[e] The First Geological Brigade of Hubei Geological Bureau, Daye 435100, PR China

ARTICLE INFO

Keywords:
Li
Nd
Sr isotope
Adakitic rock
Crust
Mantle interaction
Fractional crystallization
Middle
Lower Yangtze River Metallogenic Belt

ABSTRACT

The petrogenesis of adakitic rocks and their implications for the crust–mantle interaction remain enigmatic. To provide important insights into these issues, we carried out a detailed investigation of Li–Nd–Sr isotopes and elements for the Early Cretaceous intermediate rocks and related mafic microgranular enclaves (MMEs) from the southwestern Middle–Lower Yangtze River Metallogenic Belt, central eastern China. The intermediate rocks in the Edong district are characterized by high SiO_2, MgO, and K_2O and low Na_2O concentrations of 61.5–66.1 wt%, 0.4–2.3 wt%, 2.8–7.4 wt%, and 2.3–5.5 wt%, respectively, enrichment in LREEs and LILEs (e.g., Sr and La concentrations of 414.99–1619.45 ppm and 20.41–53.88 ppm), and relative depletion in Y (7.84–19.20 ppm) and Yb (0.59–1.73 ppm), endowed with both the high silica adakitic and high-K calc-alkaline affinities. The MME-bearing adakitic rocks exhibit wide ranges of $(^{87}Sr/^{86}Sr)_i$, $\varepsilon_{Nd}(t)$ and δ^7Li values (0.7028–0.7087, −8.9 to −3.0 and − 2.0‰ to +9.9‰, respectively), indicating a mixing process between felsic melts from a juvenile lower crust and mafic melts from an enriched mantle source. They were subsequently subjected to significant fractional crystallization of pyroxene and hornblende and minor crustal contamination during the ascent. High Sr/Y and La/Yb ratios, the salient geochemical peculiarities of adakitic rocks, might be inherited from magma sources and then be strengthened by fractionation of ferromagnesian phases. Hybrid magmas with high water content, and high oxygen and sulfur fugacity facilitate Cu ± Mo ± Au polymetallic mineralization. The adakitic rocks and related deposits in central eastern China could be related to upwelling of asthenospheric mantle caused by the subduction of the Paleo-Pacific plate during the Early Cretaceous and its induced reactivation of sub-continental lithosphere. The crust–mantle interaction model is probably applicable to formation of the adakitic rocks worldwide.

1. Introduction

Since the identification of adakite in some modern arcs (Drummond and Defant, 1990), numerous studies have recognized it as a suit of intermediate to felsic volcanic or intrusive rocks with salient geochemical and isotopic features (sodic, aluminous, $SiO_2 \geq 56$ wt%, high Sr/Y (≥40) and La/Yb (≥20), and strongly depleted in Y (≤18 ppm) and Yb (≤1.9 ppm)), originally thought to be associated with partial melting of young and hot subducted slabs (e.g., Martin, 1999; Stern and Kilian, 1996). Thereafter, newer studies on adakites or adakitic rocks do not support their affiliations with a particular convergent setting involving island arcs and continental margins (Defant et al., 1991, 1992; Evans and Hanson, 1997; Smithies and Champion, 2000). Instead, those studies suggest that adakitic rocks can also be products in the post-kinematic setting. The uncertain petrogenesis of adakitic rocks has been a first order geological problem over the past three decades (Martin et al.,

* Corresponding author at: State Key Laboratory of Petroleum Resources and Prospecting, China University of Petroleum (Beijing), Beijing 102249, PR China.
** Corresponding author at: Gemological Institute, Guilin University of Technology, Guilin 541004, PR China.
E-mail addresses: lizhuangcc@pku.edu.cn (Z. Li), jzgirlccj@163.com (C. Chen).
[1] Current address: State Key Laboratory of Petroleum Resources and Prospecting, China University of Petroleum (Beijing), Beijing 102249, China.

https://doi.org/10.1016/j.lithos.2021.106308
Received 3 March 2021; Received in revised form 16 June 2021; Accepted 16 June 2021
Available online 19 June 2021

2005). Moreover, the Cu ± Mo ± Au mineralization genetically related with adakitic rocks has extended our views from an indication of tectonic setting further to prospective for porphyry polymetallic deposits as their potentially economic benefits (Mungall, 2002; Oyarzún et al., 2001; Sajona and Maury, 1998).

The Middle–Lower Yangtze River Metallogenic Belt (hereafter referred to as the MYRMB) is an ideal natural laboratory with voluminous and well-preserved Cu–Fe–Au–Mo ore-forming or barren adakitic rocks (Fig. 1; Li et al., 2010; Pan and Dong, 1999; Wang et al., 2003; Xu et al., 2002; Zhai et al., 1996). However, the ore-forming mechanism has not been unequivocally established, largely due to a lack of understanding of reliable petrogenesis for the adakitic magmas (Wang et al., 2004, 2006; Zhou et al., 2015). Compared to adakites from modern arcs, the adakitic rocks in the MYRMB are potassium-rich, of high $Mg^{\#}$ value [molar $Mg/(Mg + Fe^{2+})$; higher than experimental melts at a given silica content], and isotopically akin to the continental crust (Rapp et al., 2003; Wang et al., 2004; Xiao and Clemens, 2007), aka C-type adakitic rocks (Xu et al., 2002). Numerous models have been proposed to account for magmatic process and the magma sources of the adakitic rocks in MYRMB. The crustal source model proposed by Wang et al. (2004) suggested that the adakitic rocks represent partial melts of delaminated lower crust at mantle depths, whereas Ling et al. (2009) argued for an oceanic crustal origin. Alternatively, it is proposed that the adakitic rocks are derived from single enriched mantle source, involving large-scale melting of metasomatized mantle peridotite (Li et al., 2008, 2009) and fractional crystallization processes of mantle-derived basaltic magmas (Li et al., 2013). More recently, Chu et al. (2020) proposed a magma mixing model between felsic melts derived from juvenile lower crust and mafic melts from enriched lithospheric mantle. The uncertainty in the petrogenesis of the adakitic rocks in the MYRMB can be deciphered by combining a systematic petrological and geochemical study, including a comprehensive overview of both radioactive and stable isotopes (Li–Nd–Sr isotopes) as well as the geochemistry of the adakitic rocks and their related mafic microgranular enclaves (MMEs), with other geological and geophysical evidence.

Therefore, in this contribution, we report new Li–Nd–Sr isotopic and elemental data and summarize the published data on the Early Cretaceous adakitic rocks and their related MMEs in the Edong district, southwestern MYRMB. To explain the geochemical and isotopic variations, we established models to simulate elemental behaviors during possible magma evolutions including mixing magmas from multiple sources, fractional crystallization, and crustal contamination processes, which provide much needed insight into the Early Cretaceous tectonic–magmatic evolution of the MYRMB.

2. Geological background and early cretaceous magmatism

Three major Precambrian blocks are recognized in China, viz. the North China, South China and Tarim cratons, separated and sutured by Phanerozoic orogenic belts (Zhao and Cawood, 2012). The North China and South China cratons are considered to have collided along the Qinling–Dabie–Su–Lu ultrahigh-pressure metamorphic belt (Wan et al., 2005). The South China Craton consists of the Yangtze Block to the northwest, the Cathaysia Block to the southeast and the east–northeast-trending Neoproterozoic Jiangnan Orogen in between (Chen et al., 2001, 2018). The basement rocks of the Cathaysia Block consist of the Paleoproterozoic gneisses and Neoproterozoic volcanic-sedimentary rocks, and those of the Jiangnan Orogen are the Shuangqiaoshan Group with greenschist-facies metamorphism dominated by the Neoproterozoic metasedimentary rocks and subordinate metavolcanic rocks (Li et al., 2013). In contrast, the Archean basement rocks in the Yangtze Block consist of amphibolites, metasedimentary rocks, tonalite–-trondhjemite–granodiorite (TTG) gneisses with amphibolite- to granulite-facies metamorphism, commonly known as the Kongling Group (Gao et al., 2011).

Along the northern margin of the Yangtze Craton, the MYRMB is bounded by the Xiangfan–Guangji Fault to the northwest, the regional strike–slip Tancheng–Lujiang Fault to the northeast, and the Yangxin–-Changzhou Fault to the south (Fig. 1; Xie et al., 2011). The MYRMB is characterized by three tectono-stratigraphic units: i.e., lowermost Proterozoic Dongling Group dominated by low-grade metasedimentary rocks and intercalated metavolcanic rocks transitional upward to the unconformably overlying Cambrian to Early Triassic submarine sedimentary rocks in the middle, and the uppermost Triassic to Cretaceous terrigenous clastic and volcanic rocks (Chen et al., 2001). Early Cretaceous magmatic rocks are concentrated in seven mining districts along the MYRMB, viz. the Edong, Jiurui, Anqing, Luzong, Tongling, Ningwu, and Ningzhen region (Fig. 1; Mao et al., 2006; Zhou et al., 2008). Late Mesozoic ore mineralization associated with more than 260 coeval intrusions with individual outcrop areas $>0.2\ km^2$ can be further divided into two types, viz. (i) the Cu–Au–Mo–Pb–Zn–(Fe) polymetallic mineralization related to Si-rich, high-K calc-alkaline rock series, and (ii) the "Daye-type" Fe (Cu, Co, and S) and "Ningwu-type" Fe (S, V, Ti, and P) mineralization related to Si-poor, high-Na calc-alkaline rock series (Fig. 1; Li et al., 2013; Zhai et al., 1992, 1996).

The Early Cretaceous magmatism in the Edong district consists of the volcanic rocks in the Jinniu basin and several associated granitoid complexes (Fig. 2; Xie et al., 2006, 2008, 2011). The granitoid complexes dated at ca. 146–120 Ma are hosted by Silurian to Early Triassic sedimentary rocks, and comprise six major plutons from north to south (Fig. 2; Li et al., 2013; Mao et al., 2006; Zhou et al., 2008): (i) the Echeng granite, monzonite, and minor quartz diorite in the southwestern part; (ii) the Tieshan quartz diorite, and minor gabbro in the southern part; (iii) the (Wangbaoshan–) Jinshandian quartz diorite in the east and diorite in the west; (iv) the Lingxiang diorite and quartz diorite; (v) the Yinzu quartz diorite; and (vi) the Yangxin quartz diorite, and minor diorite and granite porphyry (Fig. 3a, b; Xie et al., 2008). In addition, there are more than 100 small granite and granodiorite porphyry stocks, such as the Tongshankou and Fengshandong stocks, and a number of dykes (diabase, diorite, monzonite, and syenite), surrounding or intruding these batholiths or stocks. Field investigations reveal that the Lingxiang stock, and Tieshan and Yinzu batholiths contain abundant *syn*-plutonic dykes (Fig. 3c, d) and MMEs (Fig. 3e–g) of gabbroic–dioritic composition and coeval mafic dykes (Chu et al., 2020; Li et al., 2009). Detailed geology, petrology, and geochronology of the individual granitoid complexes in the Edong district refer to Chu et al. (2020), Li et al. (2009, 2010, 2013), Xie et al. (2006, 2008, 2011) and references therein (Fig. 3; Supplemental File 1).

3. Analytical methods

The samples for this contribution were collected from the Tieshan, Yinzu, and Yangxin batholiths, and the Lingxiang, Tongshankou, Fujiashan, Ruanjiawan and Fengshandong stocks (Fig. 2; Supplemental File 1). Data acquisition and results for the samples are presented in detail as Supplemental File 2 and Tables 1–2, including Li isotope measured on a Thermo Scientific Neptune Plus multiple-collector inductively coupled plasma–mass spectrometry (MC–ICP–MS) at University of Science and Technology of China, Sr—Nd isotope measurements using a Thermo-Finnigan TRITON Thermal Ionisation Mass Spectrometer (TIMS) and a MC–ICP–MS at Wuhan Sample Solution Analytical Technology Co., Ltd., and the bulk-rock composition measured with X-ray fluorescence spectrometry and inductively coupled plasma–mass spectrometry at the Wuhan Sample Solution Analytical Technology Co., Ltd. and Key Laboratory of Crustal Dynamics, Institute of Crustal Dynamics, CEA.

4. Results

The Early Cretaceous host intermediate rocks in the Edong district show a narrow range of SiO_2 (61.54–66.12 wt%) and MgO (0.42–2.36 wt%) concentrations with high $Mg^{\#}$ values (28–60, 45 on average).

They contain low concentrations of alkali metals ($Na_2O + K_2O$ = 6.46–9.74 wt%) and thus are generally classified as tonalite–quartz monzonite of subalkaline affinity in Fig. 4a (Irvine and Baragar, 1971; Middlemost, 1994), with only three outliers falling in the alkaline field. They mainly plot in the granodiorite field and near the boundary of granodiorite–granite in Fig. 4b. In addition, they are slightly metaluminous to peraluminous with A/CNK ratios ranging from 0.86 to 1.30 (1.08 on average; Fig. 4c) and plot as high-K calc-alkaline rock series with Na_2O/K_2O ratios mainly between 1 and 2 (some even below 1) (Fig. 4d). They have relatively high total Fe_2O_3 (1.72–4.68 wt%), TiO_2 (0.38–0.68 wt%), CaO (3.42–5.38 wt%), Cr (6.43–38.35 ppm) and Ni (5.00–21.46 ppm) abundances (Table 1). Compared with the host intermediate rocks, the MMEs (including mafic dykes) have a wide range of SiO_2 content (44.31–58.87 wt%) and relatively high concentrations of MgO (2.61–6.81 wt%) with high $Mg^{\#}$ values (49–59, 54 on average). The MMEs plot across the boundary between subalkaline and alkaline fields (Fig. 4a) and overlap with the host in the A/CNK–A/NK (Fig. 4c) and Na_2O–K_2O diagrams (Fig. 4d). The MMEs have high concentrations of MgO, Cr, Ni and Y (Y of 19.1–61.2 ppm) than the host intermediate rocks. The previously published data of the Early Cretaceous adakitic rocks from the Edong district (references from Chu et al., 2020; Li et al., 2009, 2010, 2013; Wang et al., 2004; Xie et al., 2006, 2008, 2011) are also shown in the following figures (Figs. 4–7) as a comparison to the present data. Taking all samples together, with MgO, CaO, total Fe_2O_3 and TiO_2 decreasing, SiO_2 and alkali metals increase, and Al_2O_3 and Na_2O/K_2O remain roughly constant (Fig. 5a–g). Compatible trace elements (Cr, Ni, and V) correlate positively with MgO (Fig. 5m–o), and no correlation can be found between most incompatible elements and MgO (e.g., Ba and Sr versus MgO in Fig. 5). All samples in this contribution have uniformed chondrite-normalized REE patterns: both the host intermediate rocks and MMEs have enriched light rare earth elements (LREEs) represented by $(La/Yb)_N$ (subscript N denotes the chondrite normalized) ratios of 7.2–34.5.7 (18.8 on average) and 9.1–42.3 (22.5 on average), respectively (Fig. 6a). They mainly show slightly negative to positive Eu anomalies in the chondrite-normalized REE patterns and negative P and Ti anomalies in primitive mantle-normalized spider diagrams (Sun and McDonough, 1989). The vast majority of the samples are enriched in large ion lithophile elements (LILEs, e.g., Rb, Sr and Ba), Zr, and Hf, but depleted in Nb and Ta (Fig. 6b).

The whole-rock Sr–Nd–Li isotopic compositions of the host intermediate rocks and MMEs are listed in Table 2. When we adopt $\varepsilon_{Nd}(t) = \varepsilon_{Nd}(0.13\ Ga)$ to discuss the characteristics of the magma sources, they all have indistinguishable Sr–Nd–Li isotopic compositions, with $(^{87}Sr/^{86}Sr)_i$ = 0.7063–0.7089, $\varepsilon_{Nd}(t)$ = −9.0 to −5.0, δ^7Li = −2.0‰ to +9.9‰ and $(^{87}Sr/^{86}Sr)_i$ = 0.7024–0.7087, $\varepsilon_{Nd}(t)$ = −8.9 to −3.0, δ^7Li = +0.86‰ to +4.6‰, respectively. Only sample HL–1 is excluded owing to its lowest $(^{87}Sr/^{86}Sr)_i$ and highest $\varepsilon_{Nd}(t)$ values (0.6997 and + 4.8). The one-stage Nd model ages (T_{DM1}) of the enclaves and their host intrusions are 1.14–1.55 Ga and 1.09–1.82 Ga with two-stage model ages (T_{DM2}) of 1.33–1.66 Ga and 1.27–1.67 Ga, respectively. The model ages appear to indicate derivation from South China Craton as Meso- to Paleoproterozoic are periods of major lithotectonic events (Chen et al., 2001, 2018; Li and McCulloch, 1996).

5. Discussion

5.1. Petrogenesis of the early cretaceous intermediate rocks in the Edong district

5.1.1. Magma mixing: multiple magma sources versus singular source

The Early Cretaceous intermediate rocks in the Edong district have high Sr (≥414 ppm) and La (≥20 ppm), and low Yb (≤1.7 ppm) and Y (≤7.8 ppm) contents, yielding relatively high Sr/Y (31.0–102.6) and $(La/Yb)_N$ (9.12–42.25) ratios, belonging to the group of adakitic rocks (Drummond and Defant, 1990), whereas the MMEs mainly plot in the classic island arc field (Fig. 7a, Fig. 7b). As aforementioned, the origin of

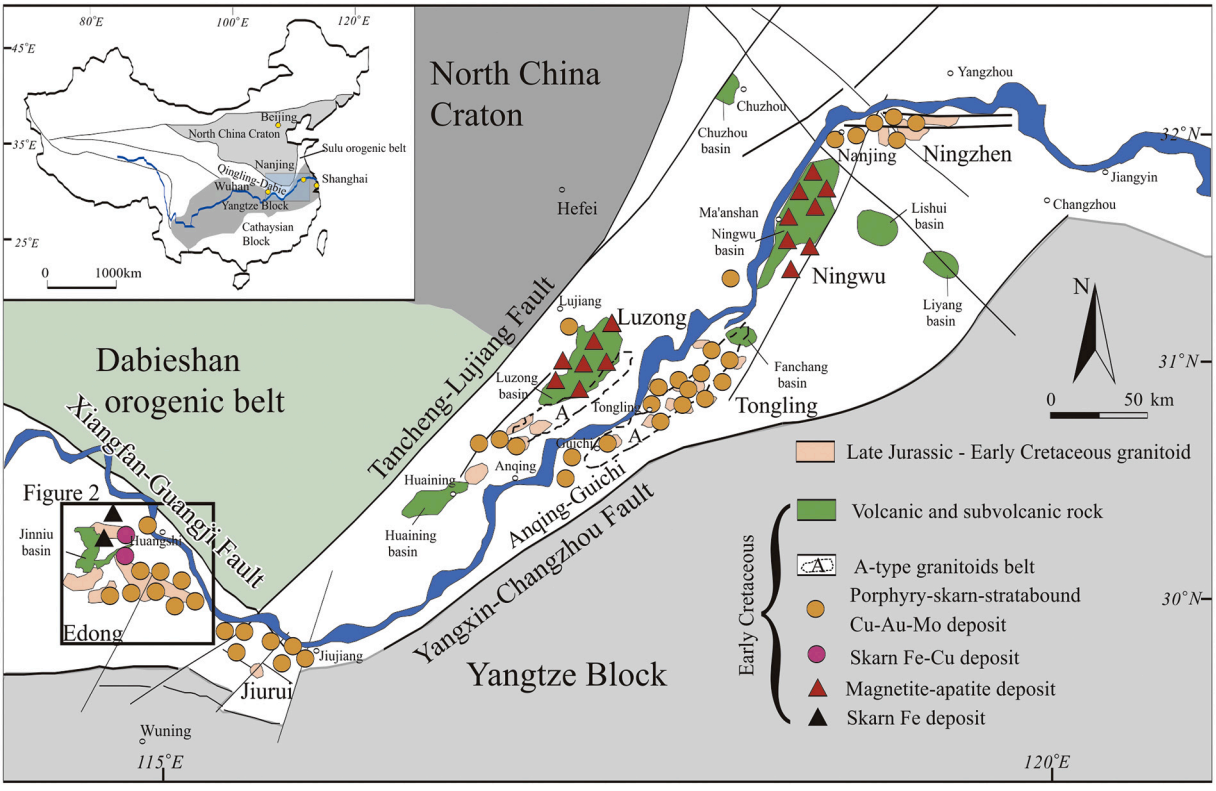

Fig. 1. Geological sketchmap showing the distribution of major Early Cretaceous granitoid plutons and related ore deposits in the MYRMB, central eastern China. Modified from Chang et al. (1991), Pan and Dong (1999), Mao et al. (2011) and Xie et al. (2011).

the Early Cretaceous adakitic rocks in the MYRMB is still an enigma (Chu et al., 2020). The adakitic rocks have been suggested to be derived from (i) partial melting of delaminated lower crust at mantle depths (Wang et al., 2003, 2004, 2006), (ii) large-scale melting of metasomatized mantle peridotite (Li et al., 2008, 2009), (iii) fractional crystallization of basaltic magmas from mantle peridotite (Li et al., 2010, 2013), (iv) partial melting of the down-going Pacific oceanic crust in the Mesozoic (Ling et al., 2009), or (v) magma mixing between mafic and felsic melts (Chen et al., 2016; Chu et al., 2020). The essential difference among those models is the magma source, viz. multiple magma sources versus singular crustal or mantle source. The following evidence is identifiable to favor magma mixing based on the existing isotope and geochemical data, whereas it still has a storm of contradictions with the remaining models.

First, and most striking of all, is the fact that the MMEs are minor but prevalent within the Early Cretaceous adakitic rocks in the Edong district, such as in the Tieshan and Yinzu batholiths, and Lingxiang stock (Chu et al., 2020; Li et al., 2009; Fig. 3). Although the MMEs can be generated via (i) early crystallization from the mafic–ultramafic magma (Noyes et al., 1983), (ii) incorporation of the residual phases from the magma source (White et al., 1999) or the country rocks during the emplacement, or (iii) mixing between externally injected mafic and the host felsic magma (Chen et al., 2009; Feeley et al., 2008; Holden et al., 1987), we favor the mixing model as it explains the evidence that the MMEs in the Edong district were quenched (Fig. 3). The fine-grained subhedral equigranular textures of the MMEs (Fig. 3d–g; Chu et al., 2020) preclude possibilities of the early crystallization from the mafic–ultramafic magma with cumulative textures and residual phases from the magma source with metamorphic textures (White et al., 1999), which was also confirmed by the occurrence of acicular apatite and elongated hornblende attributed to rapid cooling within the MMEs (Chen et al., 2016; Chu et al., 2020). The rounded to ellipsoidal shapes, no solid-state deformation and heterogeneous zone of the MMEs probably suggest stretching plastically within a convective magma, distinguished from incorporation of the country rocks during emplacement with angular shape and brittle deformation (Fig. 3e–g). The quartz ocelli surrounded by fine-grained dark mineral assemblages in the MMEs (Fig. 3e) indicates that crystal exchange between MMEs and host adakitic magma locally happened and two magmas have been co-existing for sufficient long time (Chen et al., 2009), consistent with oval in shape, sharp but partly diffusive contact to the hosts (Fig. 3f), transitional zones at contact (Fig. 3g), and back-veining (Chu et al., 2020). Crystal exchange was coupled with chemical transfer as inferred by the similar REE patterns of the MMEs and the host adakitic rocks, indicating that they are likely cogenetic (Fig. 6a). In addition, the hybrid origin of the MMEs is supported by the large variations in whole-rock chemistry, which argue for a heterogeneous mixing (Fig. 4–6; Table 1). Magma mixing between the MMEs and host adakitic rocks is also supported by the features of exchange of materials with abnormal zoning of plagioclase, with the appearance of alternating Ca-rich and Na-rich components and the outermost plagioclase zone wrapping the microcrystallites within the MMEs from the Tongling district in the vicinity of the Edong district (Chen et al., 2016). Thus, the occurrence of MMEs in the Edong district suggests that magma mixing has probably played an important role in the formation of the host adakitic rocks (Clynne, 1999; Kemp, 2004). The MMEs contain less SiO_2 (>44.13 wt%) and more Na_2O (2.82 on average), MgO (up to 6.81 wt%), Cr (19.14–311.22 ppm), Co (10.28–44.06 ppm), and Ni (10.79–202.65 ppm; Table 1)

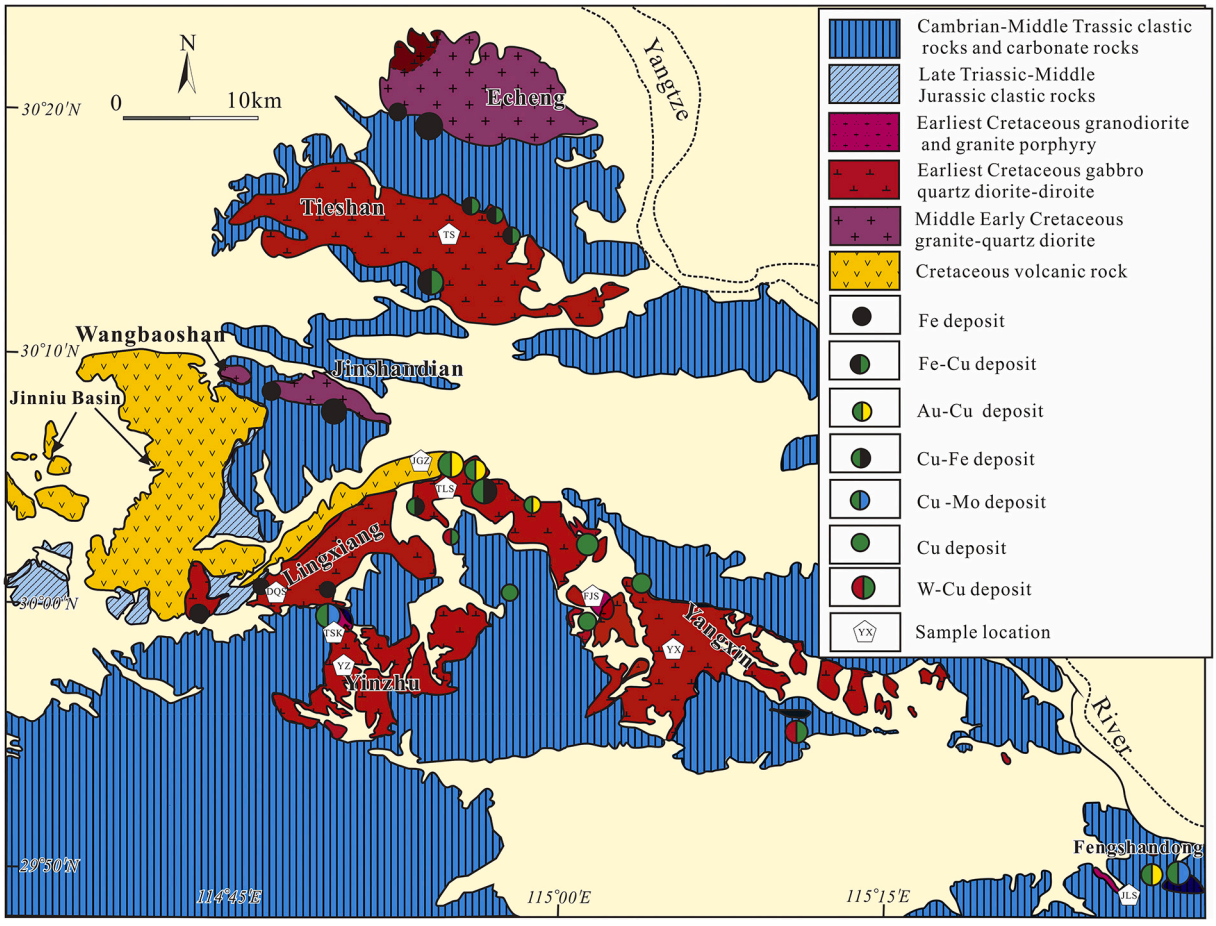

Fig. 2. Geological map of the southeastern Hubei Province, MYRMB, showing main type of mineral deposits and location of samples in this contribution. Modified from Xie et al. (2011).

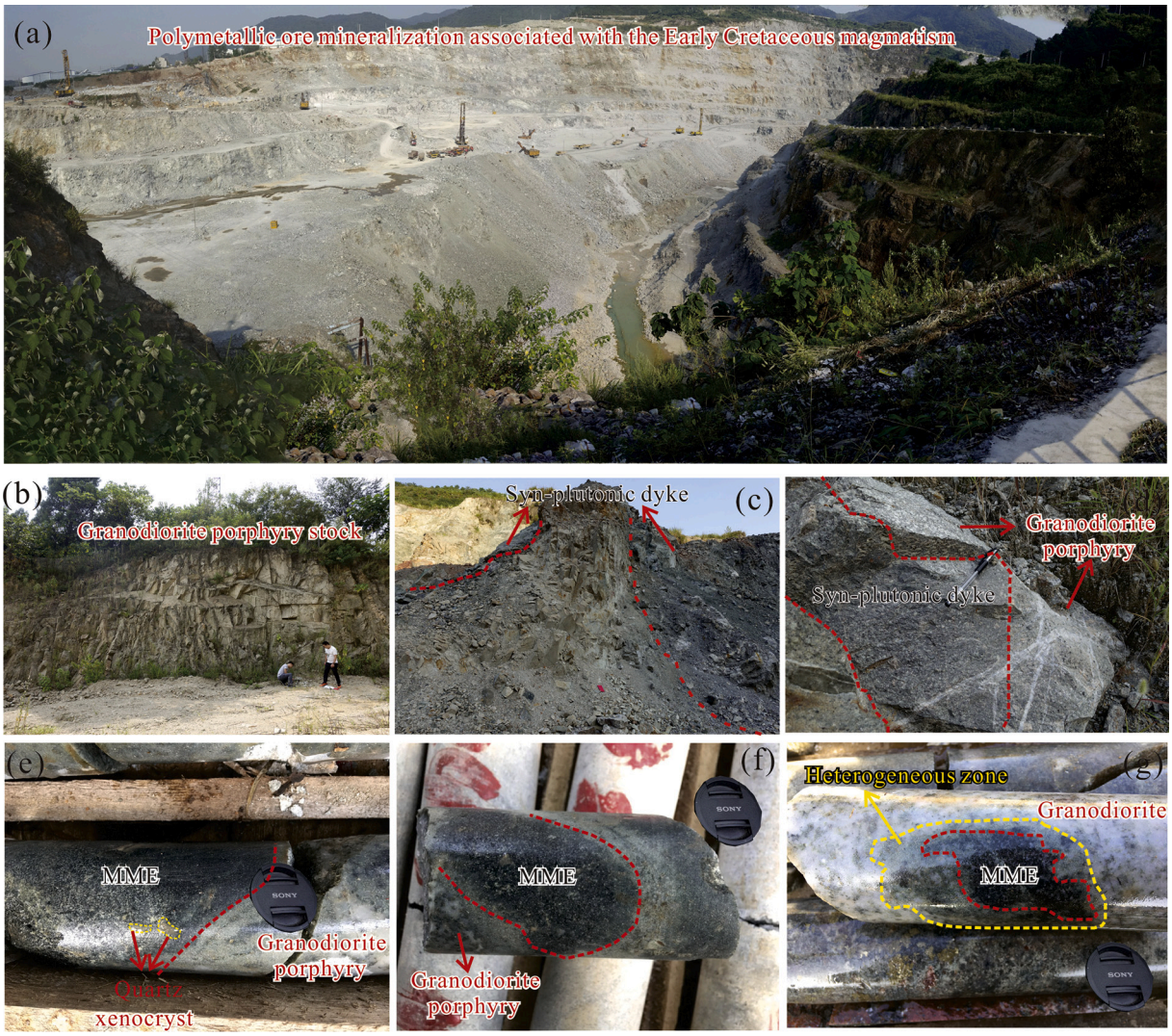

Fig. 3. (a–d) Photographs of the outcrop and (e–g) photomicrographs of the granitoid complexes in the Edong district.

contents than the crust-derived felsic melts, suggesting that the parental magma was derived mainly from a mantle source region (Frey and Prinz, 1978). However, they have also possibly recorded the significant fractional crystallization of ferromagnesian phases and magma mixing (Fig. 5), as evidenced by the fact that primary mantle-derived melts commonly have high Ni and Cr contents (>400 ppm and >1000 ppm, respectively; Wilson, 1989). A possible genetic model is that the *syn*-plutonic dykes were primarily derived from a mantle source, then evolved via fractional crystallization (Fig. 5), and finally were injected into and mixed with the host felsic magma to form the MMEs in the Edong district instead of a homogenous magma source. In such a scenario, the MMEs are the remnants after extensive magma mixing processes, so the quantity of the mafic magma during the Early Cretaceous should be greater in extent than that exposed today. The mantle source for the MMEs can provide both heat and mass to form the host adakitic rocks, whereas the nature of the mantle source was not constrained. The MMEs are characterized by significant enrichment of LREEs (Fig. 6a) and LILEs such as Sr (517–1776 ppm) and Ba (up to 1293 ppm), suggesting that they should be derived from an enriched mantle source. The pronounced negative Nb and Ta anomalies of the MMEs in the primitive mantle-normalized spidergrams (Fig. 6b) differ them from plume-related or asthenosphere-derived magmas with trace-element patterns of OIB or MORB (Hofmann, 1988, 1997). The range in $(^{87}Sr/^{86}Sr)_i$ values from the relatively unradiogenic analyses fall into the field of mafic rocks in the MYRMB trend to radiogenic counterparts (Fig. 8), indicating a continuous input of an enriched mantle (EM II). The EMII trend was also recognized in the MMEs at Dexing in the vicinity of the Edong district (Hou et al., 2013), which overlaps with the basalts in the Society Islands that were derived from EMII (Fig. 7; Hawkesworth et al., 1984). Sr—Nd isotope and multiple geochemical proxies, especially the continuous variations in elements, parallel REE, and spider patterns (Fig. 6), indicate that the MMEs and Mesozoic mafic rocks in MYRMB shared one EMII source even if the MMEs might be contaminated by the host adakitic rocks and experience significant fractional crystallization during emplacement, that is cogenetic products of common parental magmas. The abundance of euhedral hornblende crystals in the MMEs also reveals hydrous nature of the parental magma, which suggests a hydrous mantle source metasomatized by subduction recycling of sediment (EMII; Schmidt et al., 2004; Tasumi et al., 1986; Xie et al., 2006; Zhou et al., 2008). The most 'primitive' isotopic compositions of the MMEs (Table 2), which is considerably less radiogenic than that of depleted asthenospheric mantle at this time, suggest a long-term enriched sub-continental lithospheric mantle origin for it rather than derivation from the Mesozoic mantle metasomatism by the Paleo-Pacific subduction zone fluid/melt alone, and thus for all the MMEs of this study (e.g., Jahn et al., 1999).

Second is the whole-rock geochemistry. The $Mg^{\#}$ values (28–60) and MgO contents (3.42–5.38 wt%) of the Early Cretaceous adakitic rocks in

Table 1
Chemical data.

Sample	Mafic dyke		Mafic microgranular enclave			Host diorite and quartz diorite																		
No.	TLS-6	HL-1	TSK-5	YZ-5	JLS-1	TLS-1	TLS-2	TLS-4	TLS-5	TLS-7	JGZ-1	DQS-1	YX-4	YX-5	YX-6	DQS-1-1	FJS-1	RJW-1	TS-2	TS-3	JLS-2	JLS-3	JLS-4	JLS-5	JLS-8
SiO_2 (wt%)	44.31	49.25	59.87	59.30	59.13	66.12	63.25	62.80	63.47	62.40	63.07	61.96	62.21	64.66	64.51	63.45	65.87	64.41	61.54	64.57	63.76	63.61	63.51	63.97	62.98
TiO_2	2.55	1.94	0.88	0.74	0.60	0.41	0.38	0.54	0.50	0.67	0.53	0.55	0.57	0.57	0.57	0.55	0.44	0.47	0.68	0.54	0.55	0.54	0.50	0.62	0.57
Al_2O_3	12.66	14.09	14.46	16.20	15.74	15.54	15.23	15.92	16.27	16.34	16.31	16.15	16.72	16.07	16.20	16.09	15.26	15.84	16.60	16.14	15.29	15.02	14.06	15.38	15.78
Fe_2O3_T	12.13	10.17	5.84	6.58	3.57	1.72	2.28	4.32	3.00	4.54	3.97	3.87	3.37	4.43	4.43	4.42	3.56	3.91	3.87	3.62	2.90	3.21	2.56	4.53	4.68
MnO	0.16	0.14	0.10	0.12	0.10	0.04	0.04	0.09	0.05	0.09	0.06	0.07	0.03	0.10	0.10	0.09	0.06	0.08	0.07	0.06	0.06	0.08	0.08	0.07	0.03
MgO	5.21	6.18	3.67	3.21	2.61	0.42	1.33	1.48	1.19	2.01	0.78	0.87	1.11	1.63	1.57	1.51	1.54	1.69	1.80	1.37	2.06	2.23	1.97	2.36	1.73
CaO	14.62	8.45	4.87	5.83	6.08	3.42	3.82	5.38	5.25	4.57	4.92	5.38	4.98	4.55	4.64	4.74	3.63	3.86	4.96	3.54	4.66	4.53	4.90	3.76	3.49
Na_2O	1.05	2.93	3.60	3.33	3.22	4.22	3.31	4.29	4.50	4.53	4.16	4.41	4.52	4.10	4.28	4.23	4.14	4.00	5.48	5.22	4.74	3.62	2.31	3.87	3.55
K_2O	5.33	1.17	3.67	2.87	5.91	4.37	3.65	2.90	3.59	3.30	3.14	2.95	3.16	2.95	2.93	2.92	3.11	2.81	3.16	3.12	3.73	5.19	7.43	2.92	2.91
P_2O_5	1.98	0.34	0.37	0.36	0.19	0.19	0.17	0.27	0.22	0.30	0.25	0.26	0.26	0.27	0.28	0.26	0.21	0.23	0.29	0.22	0.17	0.18	0.17	0.24	0.18
LOI	0.90	4.82	2.13	0.98	2.33	3.53	6.04	1.51	1.43	0.74	2.32	2.91	2.54	0.62	0.44	1.22	1.66	2.16	1.05	1.09	1.58	1.74	2.51	2.24	3.58
Total	100.90	99.47	99.45	99.51	99.48	99.98	99.50	99.49	99.47	99.49	99.51	99.38	99.47	99.96	99.95	99.48	99.48	99.46	99.49	99.49	99.49	99.95	100.00	99.96	99.49
K_2O/Na_2O	5.87	0.40	1.02	0.86	1.84	1.04	1.10	0.68	0.80	0.73	0.75	0.67	0.70	0.72	0.68	0.69	0.75	0.70	0.58	0.60	0.79	1.43	3.22	0.75	0.82
$K_2O + Na_2O$	6.38	4.10	7.27	6.20	9.13	8.59	6.96	7.19	8.09	7.83	7.30	7.36	7.68	7.05	7.21	7.15	7.25	6.81	8.64	8.34	8.47	8.81	9.74	6.79	6.46
$Mg^{\#}$	0.53	0.55	0.55	0.49	0.59	0.32	0.54	0.40	0.44	0.47	0.28	0.31	0.39	0.42	0.41	0.40	0.46	0.46	0.48	0.43	0.58	0.58	0.60	0.51	0.42
A/CNK	0.70	1.02	1.01	1.17	0.91	1.05	1.18	1.05	1.01	1.08	1.11	1.05	1.09	1.14	1.12	1.11	1.13	1.21	0.98	1.06	0.95	0.96	0.86	1.19	1.30
A/NK	1.95	2.31	1.46	1.89	1.35	1.33	1.62	1.56	1.44	1.48	1.59	1.55	1.54	1.62	1.59	1.59	1.50	1.65	1.33	1.35	1.29	1.30	1.19	1.61	1.76
CaO/Na_2O	16.10	2.88	1.35	1.75	1.89	0.81	1.15	1.25	1.17	1.01	1.18	1.22	1.10	1.11	1.08	1.12	0.88	0.97	0.91	0.68	0.98	1.25	2.12	0.97	0.98
Li (ppm)	21.31	8.354	18.39	19.90	9.342	7.581	12.60	8.065	7.986	10.46	11.18	14.05	10.44	18.73	21.02	13.00	13.31	17.81	12.57	12.37	10.06	9.982	6.429	26.01	12.66
Be	4.657	1.242	3.025	2.114	1.795	1.638	1.711	2.378	2.279	2.383	2.342	2.205	2.407	2.335	2.365	2.579	2.370	2.313	2.594	2.641	1.979	1.652	1.341	1.944	1.688
P	8659	1466	1597	1554	820.4	842.2	733.1	1156	977.5	1318	1100	1113	1126	1196	1222	1143	898.9	994.9	1244	946.9	737.5	789.9	724.4	1043	802.9
Sc	22.35	19.69	11.02	14.74	9.901	3.955	3.761	6.535	5.927	7.112	5.997	6.699	6.034	6.425	6.428	6.280	5.944	6.349	6.287	5.204	9.571	9.553	8.283	8.761	7.653
Ti	15,281	11,627	5250	4405	3578	2463	2301	3207	2973	3986	3165	3308	3428	3410	3428	3266	2643	2835	4076	3254	3266	3242	3021	3710	3428
V	218.5	173.6	121.8	126.8	86.81	43.51	41.09	72.75	67.91	83.01	73.26	73.22	79.68	74.43	70.24	72.45	66.56	61.81	77.24	59.72	84.63	79.32	70.41	93.76	86.76
Cr	311.2	138.2	39.07	34.45	19.14	10.96	9.868	7.062	7.450	9.855	6.527	7.155	10.84	7.414	7.512	6.426	20.81	12.73	21.09	20.32	17.14	16.43	15.27	38.35	15.50
Mn	1269	1061	759.0	929.3	805.4	294.3	317.5	681.5	379.5	712.5	456.9	518.9	224.6	797.7	782.2	697.0	464.7	619.6	511.1	426.0	464.7	635.1	619.6	573.1	247.8
Co	44.06	42.28	20.43	19.17	10.28	3.141	6.110	8.443	5.923	8.778	8.217	7.143	9.080	8.601	8.393	8.122	10.75	8.667	11.66	7.988	7.458	8.865	7.288	13.26	9.606
Ni	202.7	109.0	25.47	15.21	10.79	9.201	10.11	5.835	5.823	7.346	5.727	5.004	8.976	5.922	5.761	5.470	12.68	9.943	19.29	12.30	9.182	9.555	8.597	21.46	8.637
Cu	83.61	64.17	2840	41.84	240.0	2.478	13.37	10.39	17.73	20.13	24.15	4.698	71.37	3.727	2.947	4.323	74.11	5.620	28.67	5.834	18.47	50.29	194.5	22.93	96.10
Zn	169.0	111.3	71.08	49.52	57.91	39.82	22.66	44.58	25.02	41.62	40.48	42.89	31.28	44.60	45.29	45.02	35.16	49.29	45.58	51.91	30.39	44.41	38.54	59.01	29.94
Ga	21.00	20.52	21.78	19.38	20.12	19.35	19.86	20.91	20.89	21.04	21.08	20.97	21.65	20.82	20.74	20.68	20.19	19.39	25.06	24.14	17.20	18.97	16.86	21.07	20.48
Rb	186.4	20.81	116.2	119.0	94.42	164.2	159.5	85.02	87.58	92.95	105.9	91.13	76.65	96.45	102.9	90.72	117.7	104.6	68.52	79.80	74.04	96.36	108.5	77.69	72.69
Sr	1775.5	517.0	846.8	757.4	852.9	415.0	573.2	1060.5	1054.7	941.5	994.5	947.5	948.5	965.2	973.5	985.5	974.3	782.1	1619.5	1267.5	844.9	699.6	841.6	753.7	525.5
Y	28.91	22.02	17.22	16.05	18.54	8.213	7.838	16.57	14.71	19.20	13.54	16.36	14.25	16.14	16.23	15.44	12.19	14.42	15.78	14.39	17.83	18.86	15.25	14.61	16.95
Zr	432.4	141.2	217.9	154.0	179.2	151.3	156.7	178.0	172.3	190.1	166.5	170.2	194.8	181.5	178.8	164.9	175.7	159.3	227.8	232.0	164.7	177.5	148.3	158.8	157.1
Nb	42.45	22.39	14.89	10.76	15.99	9.61	9.82	16.75	14.58	19.72	15.54	17.30	14.19	17.62	19.45	16.75	10.65	13.87	14.28	13.86	15.22	15.08	13.62	11.34	16.04
Sn	2.393	1.410	1.653	1.146	2.241	0.7033	0.692	1.043	0.853	1.236	0.8921	0.9660	0.6450	0.9903	0.9910	0.8911	1.008	0.9105	1.270	1.165	1.594	1.906	1.772	1.039	1.418
Cs	35.90	0.6208	3.070	4.355	0.7676	2.951	4.440	0.8285	0.7370	3.330	3.045	2.383	1.898	1.691	1.361	1.596	1.964	2.731	0.8278	1.478	1.467	1.008	0.8032	1.099	2.611
Ba	1293	232.3	824.3	1256	1032	771.3	793.4	788.1	971.3	804.0	826.2	826.7	856.4	785.5	883.7	865.1	1144	989.8	1225	938.7	774.7	859.3	1292.8	857.9	809.1
La	100.6	17.51	60.27	26.79	35.27	38.44	36.83	48.78	44.63	53.88	43.43	48.47	45.51	47.52	48.54	45.86	45.97	39.74	53.08	44.13	26.08	36.45	20.41	29.15	30.07
Ce	231.4	37.25	115.67	50.73	69.35	68.58	67.07	92.16	86.41	106.02	81.02	91.68	79.19	90.37	92.10	87.35	88.91	76.50	99.68	85.72	53.95	71.23	44.19	61.18	61.67
Pr	28.10	4.717	12.869	5.527	7.647	7.116	6.822	9.931	9.501	11.571	8.557	10.167	8.686	9.757	10.006	9.474	9.454	8.120	11.035	9.290	5.945	7.698	5.024	6.968	6.855
Nd	105.9	21.09	46.64	21.59	28.41	24.97	24.14	36.64	34.84	42.41	32.35	37.61	32.82	35.48	35.96	35.66	35.46	30.48	41.41	34.84	23.31	28.98	19.31	26.98	25.61
Sm	16.55	5.634	7.763	4.493	5.222	3.963	3.760	6.510	6.259	7.292	5.634	6.648	5.752	6.182	6.100	5.999	5.713	5.042	7.211	6.267	4.497	5.182	4.092	5.028	4.938
Eu	3.842	1.815	1.851	1.385	1.210	0.961	1.008	1.693	1.525	1.836	1.518	1.672	1.496	1.510	1.560	1.570	1.287	1.366	1.899	1.488	1.112	1.217	0.926	1.316	1.228
Gd	10.70	5.447	5.093	3.709	4.182	2.470	2.549	4.541	4.301	5.492	4.205	4.515	4.042	4.168	4.497	4.169	3.630	3.671	4.856	4.277	3.818	4.068	3.260	4.002	3.882
Tb	1.252	0.8555	0.6377	0.5380	0.6009	0.2900	0.2990	0.5789	0.5394	0.6997	0.5007	0.5769	0.5532	0.5855	0.5709	0.5771	0.4528	0.4743	0.6319	0.5798	0.5701	0.5929	0.4663	0.5273	0.5645
Dy	6.227	4.854	3.313	2.976	3.534	1.609	1.567	3.013	2.798	3.641	2.641	3.087	2.690	3.073	3.175	3.002	2.428	2.737	3.125	2.805	3.234	3.308	2.852	2.868	3.185
Ho	1.035	0.8349	0.5626	0.5814	0.6339	0.2983	0.2638	0.5607	0.5084	0.6685	0.4562	0.5841	0.5009	0.5679	0.5575	0.5217	0.4281	0.4874	0.5724	0.5196	0.6192	0.6633	0.5538	0.5125	0.6318
Er	3.015	2.042	1.606	1.583	1.846	0.814	0.754	1.610	1.383	1.860	1.265	1.530	1.378	1.476	1.555	1.495	1.255	1.291	1.462	1.394	1.678	1.807	1.484	1.284	1.674
Tm	0.3781	0.2776	0.2239	0.2336	0.2643	0.1130	0.0995	0.2324	0.2054	0.2777	0.1775	0.2268	0.1880	0.2375	0.2309	0.2106	0.1672	0.1900	0.2186	0.1807	0.2725	0.2596	0.2267	0.1985	0.2709

(*continued on next page*)

Table 1 (*continued*)

Sample	Mafic dyke		Mafic microgranular enclave			Host diorite and quartz diorite																
No.	TLS-6	HL-1	TSK-5	YZ-5	JLS-1	TLS-1	TLS-2	TLS-4	TLS-5	TLS-7	JGZ-1	DQS-1	YX-4	YX-5	YX-6	DQS-1-1	FJS-1	RJW-1	TS-2	TS-3	JLS-2	JLS-3	JLS-4	JLS-5	JLS-8
Yb	2.269	1.648	1.500	1.524	1.809	0.663	0.588	1.366	1.318	1.731	1.170	1.448	1.246	1.486	1.537	1.356	1.070	1.277	1.382	1.231	1.705	1.709	1.509	1.253	1.556
Lu	0.3166	0.2068	0.2169	0.2488	0.2658	0.1025	0.0875	0.2066	0.2056	0.2654	0.1827	0.2251	0.1922	0.2320	0.2592	0.2104	0.1604	0.2069	0.2003	0.1786	0.2502	0.2582	0.2140	0.1645	0.2348
Hf	10.22	3.558	5.535	3.736	4.789	3.727	3.758	4.468	4.093	4.738	4.072	4.344	4.942	4.592	4.419	4.165	4.388	4.125	5.574	5.735	4.380	4.575	3.859	4.196	4.264
Ta	2.065	1.338	0.8125	0.5939	1.038	0.6075	0.6087	0.9283	0.8200	1.1816	0.8539	1.002	0.7923	1.045	1.095	0.9747	0.6232	0.9711	0.6939	0.7978	1.013	0.9492	0.9033	0.7095	1.012
Pb	25.12	2.664	10.320	8.667	10.10	7.307	6.804	10.10	7.342	8.418	9.110	11.66	12.67	8.520	8.829	9.196	10.36	11.75	11.30	11.70	6.632	9.045	5.690	13.10	11.35
Th	10.03	2.482	15.72	4.362	8.799	10.01	10.22	12.51	10.28	15.48	13.74	12.52	13.43	11.02	12.66	12.03	14.01	10.96	8.904	9.071	6.543	8.364	5.526	8.539	7.068
U	1.323	0.5702	5.045	1.313	1.864	2.164	4.010	2.652	2.289	3.168	3.185	2.628	2.886	2.931	2.976	3.096	3.462	2.811	2.150	2.263	1.763	1.867	1.531	2.023	2.053
TREE	511.6	104.2	258.2	121.9	160.2	150.4	145.8	207.8	194.4	237.6	183.1	208.4	184.2	202.6	206.6	197.5	196.4	171.6	226.8	192.9	127.0	163.4	104.5	141.4	142.4
Nb/Ta	23.7	16.7	18.3	18.1	15.4	15.8	16.1	18.0	17.8	16.7	18.2	17.3	17.9	16.9	17.8	17.2	17.1	14.3	20.6	17.4	15.0	15.9	15.1	16.0	15.8
Sr/Y	70.9	23.5	49.2	47.2	46.0	50.5	73.1	64.0	71.7	49.0	73.4	57.9	66.6	59.8	60.0	63.8	79.9	54.2	102.6	88.1	47.4	37.1	55.2	51.6	31.0
$(La/Yb)_N$	34.5	7.2	27.1	11.9	13.1	39.1	42.3	24.1	22.8	21.0	25.0	22.6	24.6	21.6	21.3	22.8	29.0	21.0	25.9	24.2	10.3	14.4	9.1	15.7	13.0
Eu/Eu*	0.96	0.99	0.85	1.01	0.77	0.88	0.94	0.90	0.85	0.85	0.92	0.88	0.90	0.86	0.87	0.91	0.81	0.93	0.93	0.83	0.80	0.78	0.75	0.87	0.83
$(La/Sm)_N$	4.41	1.95	4.88	3.75	4.25	6.10	6.16	4.71	4.48	4.65	4.85	4.59	4.98	4.83	5.00	4.81	5.06	4.96	4.63	4.43	3.65	4.43	3.14	3.65	3.83
$(Gd/Yb)_N$	4.39	2.67	2.74	1.96	1.87	3.00	3.50	2.68	2.63	2.56	2.90	2.52	2.62	2.26	2.36	2.48	2.74	2.32	2.84	2.80	1.81	1.92	1.74	2.58	2.01

Mg# = 100 × molar Mg/(Mg + Fe) (FeO_T = 0.8998 × Fe_2O_3); LOI = loss on ignition; A/CNK = molar $Al_2O_3/(CaO + Na_2O + K_2O)$; A/NK = molar $Al_2O_3/(Na_2O + K_2O)$.
Eu/Eu* = $Eu_N/[\sqrt{(Sm_N * Gd_N)}]$; $(La/Yb)_N$, $(La/Sm)_N$ and $(Gd/Yb)_N$, N = chondrite normalized to values of Sun and McDonough (1989); TREE = La + Ce + Pr + Nd + Sm + Eu + Gd + Tb + Dy + Ho + Er + Tm + Yb + Lu.

the MYRMB are higher than those of experimental melts from basalts at the same silica contents (Fig. 9a; Martin et al., 2005), mainly plotting in HMA (high magnesian andesite) – HSA (high silica adakite) field (Fig. 9b; Kelemen et al., 2003; Rapp et al., 2003; Rapp and Watson, 1995). Melting of lower crustal source rocks (e.g., eclogite and amphibolite eclogite) will produce melts with low $Mg^{\#}$ values ($Mg^{\#}$ < 40; Rapp and Watson, 1995; Rapp et al., 2003) and peraluminous compositions (e.g., Qian and Hermann, 2013), which is contradictory to the Early Cretaceous adakitic rocks in the Edong district. It rules out the possibility that partial melting of thickened lower crusts alone can explain the origin of these plutons (Rapp et al., 2003; Wang et al., 2003, 2004, 2006; Xu et al., 2002). An additional relatively high-Mg mafic magma likely originated from the sub-continental lithospheric mantle or even asthenospheric mantle is required (Fig. 9b; e.g., dyke sample HL–1 with pronounced positive $\varepsilon_{Nd}(t)$ value and Nb, Ta and Ti anomalies). To overcome the difficulty of the high MgO contents and $Mg^{\#}$ values (Fig. 9), Wang et al. (2004) proposed a delamination model, that is, the underlying lithospheric mantle imparts its enriched isotopic signature to the crustal melt from the thickened crust with residual garnet. However, other difficulties still exist, for example, no such lower crustal eclogites or garnet-bearing assemblages within the Cretaceous basalts in the MYRMB (Li et al., 2009) and no evidence for fractional crystallization of amounts of garnet (Fig. 10). Thus, the addition of relatively high-Mg mafic magma should not be directly interacted with the mantle but injection of the mantle derived mafic magma, which is consistent with the widespread occurrence of the MMEs within the Early Cretaceous host adakitic rocks and coeval mafic dykes in the Edong district. Analogous cases from adjacent regions have also been reported in recent years (Chen et al., 2009), in which high $Mg^{\#}$ values were believed to be related with addition of mafic magmas. The lack of correlation between MgO and Sr in the Edong district (Fig. 5q) suggests that the high LILEs contents were inherited from not only basaltic magmas derived from a lithospheric mantle that had previously been metasomatized by fluids issuing from a subducted oceanic slab, but also the crustal melts. If the adakitic signatures of the host intermediate rocks were generated mainly by the delamination or fractional crystallization, it will show a significant positive correlation between Sr/Y ratio and SiO_2 (Fig. 5r). The mixing process is also recorded by the plagioclase phenocryst within the coeval adakitic rocks from the Tongling district in the northern MYRMB, with a sodic core abruptly surrounded by a relatively Ca-rich plagioclase overgrowth and a low-Ca plagioclase in the rim (Chen et al., 2016). The low-Ca core formed in a felsic melt, and the relatively high-Ca overgrowth could result from input of mafic magma, which well matched with a process of mixing between felsic and mafic magmas (Chen et al., 2009; Clynne, 1999; Kemp, 2004), commonly observed in many other plutons related with magma mixing (e.g., Aolunhua adakitic porphyry complex from the eastern Central Asian Orogenic Belt, northern China; Ma et al., 2013).

The third line of evidence is the isotopic variations. The Early Cretaceous adakitic rocks in the MYRMB have an exceedingly large variation in the bulk-rock Nd–Sr–Li isotope (Table 2; Fig. 8; Fig. 11), as well as Hf—O isotope (Chu et al., 2020; Li et al., 2013). This also indicates that the adakitic rocks are not derived from a relatively homogeneous pristine source, but instead supports a petrogenetic model dominated by magma mixing (Griffin et al., 2002). Similar cases are also recognized in the Tongling district where the zircon $\varepsilon_{Hf}(t)$ values (−9.5 to −26.3) of quartz monzodiorite and granodiorite show significant variations (Chen et al., 2016), which argues against a closed system behavior during the evolution of the magma (Kemp and Hawkesworth, 2006). One end-member for magma mixing is the mantle-derived mafic magma as the aforementioned represented by the parental magma of the MMEs, and the other end-member should be crustal melts. Crustal melts can be derived from either Archean basement rocks beneath the study area including late Archean TTG gneisses and mafic granulites/amphibolites (Chen et al., 2001), or juvenile mafic underplating lower crust. Experimental petrology and pseudosection calculations indicate

Table 2
Li-Nd-Sr isotopic data.

Sample	Rb	Sr	$^{87}Rb/$	$^{87}Sr/$	2σ	I_{Sr}	Sm	Nd	$^{147}Sm/$	$^{143}Nd/$	2σ	$\varepsilon_{Nd}(0)$	$f_{Sm/Nd}$	$\varepsilon_{Nd}(T)$	T_{DM1}	T_{DM2}	Li	δ^7Li	2σ
No.	(ppm)	(ppm)	^{86}Sr	^{86}Sr			(ppm)	(ppm)	^{144}Nd	^{144}Nd					(Ga)	(Ga)	(ppm)		
Mafic dyke/microgranular enclave																			
TLS-6	92.95	941.5	0.2863	0.706844	9	0.70631	7.29	42.41	0.1039	0.512217	2	−8.2	−0.47	−6.7	1.29	1.47	19.97	0.86	0.11
HL-1	20.81	517.03	2.8134	0.704855	5	0.69966	5.63	21.1	0.1082	0.512708	3	1.4	−0.45	2.8	0.64	0.69	10.60	0.99	0.17
TSK-5	116.17	846.8	0.3979	0.707053	5	0.70632	7.76	46.64	0.1006	0.512302	3	−6.6	−0.49	−5.0	1.14	1.33	21.13	3.64	0.05
YZ-5	76.65	948.5	0.2344	0.709347	8	0.70891	5.75	32.82	0.1059	0.512171	2	−9.1	−0.46	−7.6	1.38	1.54	18.14	2.67	0.01
JLS-1	94.4	852.95	0.3210	0.708852	5	0.70826	5.22	28.41	0.1111	0.512103	3	−10.4	−0.44	−9.0	1.55	1.66	7.73	4.58	0.06
Host diorite and quartz diorite																			
TLS-1	164.25	415.0	1.1478	0.708768	5	0.70665	3.96	24.97	0.0960	0.512164	5	−9.2	−0.51	−7.6	1.28	1.54	7.83	8.52	0.06
TLS-2	159.47	573.2	0.8069	0.707859	7	0.70637	3.76	24.14	0.0941	0.51217	4	−9.1	−0.52	−7.4	1.25	1.53	13.63	0.79	0.10
TLS-3	85.02	1060.5	0.2325	0.707409	9	0.70698	6.51	36.64	0.1074	0.512137	4	−9.8	−0.45	−8.3	1.45	1.60	8.50	5.52	0.02
TLS-4	87.58	1054.7	0.2408	0.706238	9	0.70579	6.26	34.84	0.1086	0.512274	3	−7.1	−0.45	−5.6	1.27	1.38	8.42	5.57	0.08
TLS-5	161.56	1539.0	0.3044	0.7061	6	0.70551	14.34	91.82	0.0944	0.512293	4	−6.7	−0.52	−5.0	1.09	1.33	8.02	2.99	0.02
TLS-7	105.93	994.5	0.3089	0.706508	8	0.70594	5.63	32.35	0.1053	0.51224	3	−7.8	−0.46	−6.2	1.28	1.43	11.54	1.85	0.02
JGZ-1	91.13	947.5	0.2789	0.706291	5	0.70578	6.65	37.61	0.1069	0.512286	4	−6.9	−0.46	−5.4	1.23	1.36	12.98	5.42	0.01
DQS-1	119.01	757.4	0.4557	0.706285	6	0.70544	4.49	21.59	0.1258	0.512282	6	−6.9	−0.36	−5.8	1.50	1.39	13.30	4.16	0.08
YX-4	96.45	965.2	0.1775	0.706241	9	0.70591	6.182	35.48	0.0949	0.512285	11	−6.9	−0.52	−5.2	1.11	1.35	12.78	−2.01	0.06
YX-5	102.86	973.5	0.2339	0.706396	5	0.70596	6.10	36.0	0.0927	0.512239	5	−7.8	−0.53	−6.1	1.15	1.42	19.81	2.51	0.03
YX-6	90.72	985.52	0.5675	0.706421	6	0.70537	6.00	35.7	0.0910	0.512219	4	−8.2	−0.54	−6.4	1.16	1.45	22.46	3.44	0.08
DQS-1	117.69	974.32	0.2005	0.706241	8	0.70587	5.71	35.46	0.1037	0.512261	8	−7.4	−0.47	−5.8	1.23	1.40	13.02	5.68	0.00
FJS-1	104.63	782.08	0.1615	0.706857	6	0.70656	5.04	30.48	0.1051	0.512296	2	−6.7	−0.47	−5.2	1.20	1.34	13.74	−0.73	0.08
RJW-1	68.52	######	0.1846	0.707810	7	0.70747	7.21	41.4	0.1014	0.512281	10	−7.0	−0.48	−5.4	1.18	1.36	17.82	−0.12	0.01
TS-2	79.80	######	2.5383	0.707158	5	0.70247	6.27	34.8	0.1133	0.512097	4	−10.6	−0.42	−9.2	1.60	1.67	12.67	4.60	0.10
JLS-2	74.0	844.92	0.2541	0.708814	8	0.70834	4.50	23.31	0.1166	0.512120	9	−10.1	−0.41	−8.8	1.61	1.64	10.80	9.87	0.04
JLS-3	96.4	699.64	0.3994	0.709209	4	0.70847	5.18	28.98	0.1081	0.512110	3	−10.3	−0.45	−8.8	1.50	1.64	10.28	3.23	0.09
JLS-4	108.5	841.64	0.3737	0.708911	6	0.70822	4.09	19.31	0.1281	0.512125	4	−10.0	−0.35	−8.9	1.82	1.64	7.09	6.02	0.02
JLS-5	77.7	753.66	0.2989	0.707322	5	0.70677	5.03	26.98	0.1126	0.512345	7	−5.7	−0.43	−4.3	1.21	1.27	27.18	6.37	0.09
JLS-8	72.7	525.50	0.4012	0.709458	4	0.70872	4.94	25.61	0.1166	0.512121	4	−10.1	−0.41	−8.8	1.61	1.63	11.38	2.81	0.06

$\varepsilon_{Nd} = ((^{143}Nd/^{144}Nd)_s/(^{143}Nd/^{144}Nd)_{CHUR} - 1) \times 10{,}000$, $f_{Sm/Nd} = (^{147}Sm/^{144}Nd)_s/(^{147}Sm/^{144}Nd)_{CHUR} - 1$, $(^{143}Nd/^{144}Nd)_{CHUR} = 0.512638$, and $(^{147}Sm/^{144}Sm)_{CHUR} = 0.1967$. The model ages were calculated using a linear isotopic ratio growth equation in Chen et al. (2001).

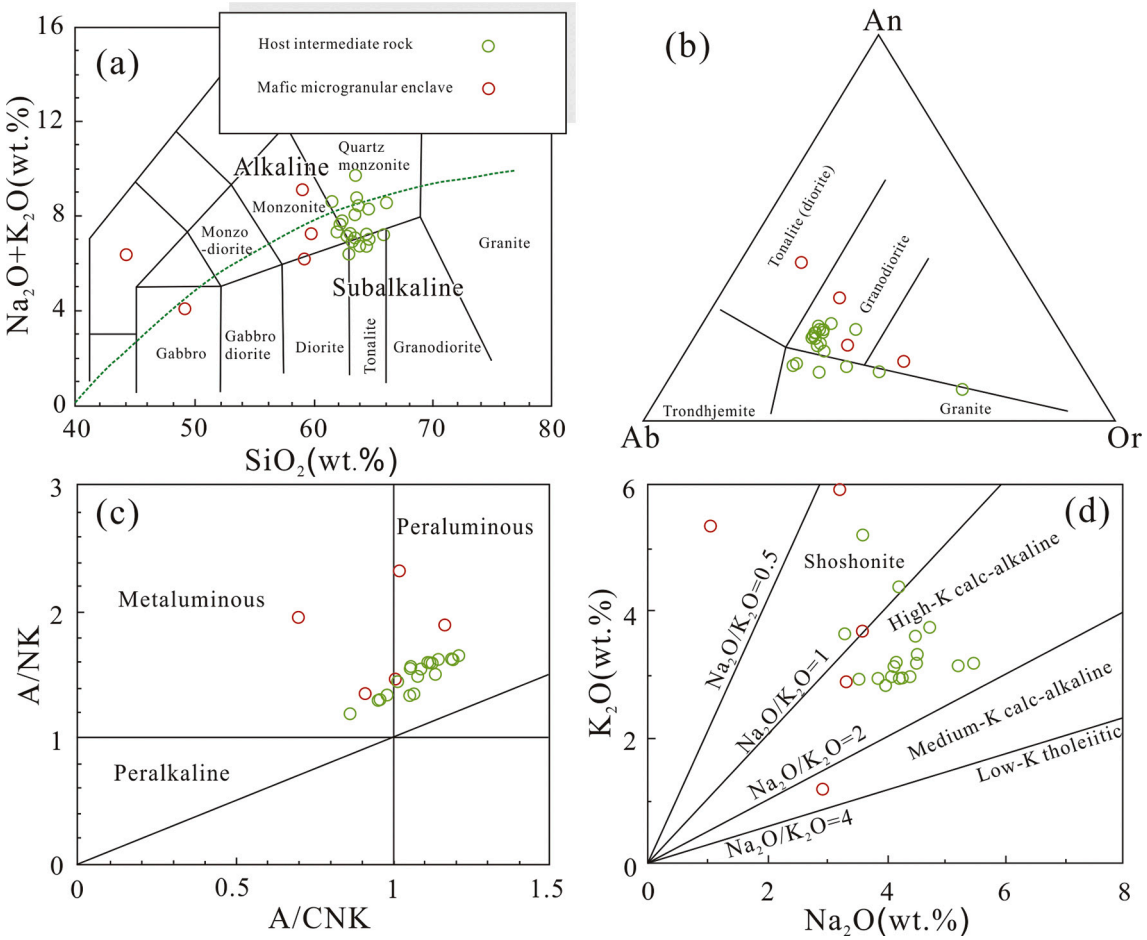

Fig. 4. Diagrams of (a) total alkalis versus SiO_2, (b) Ab–An–Or, (c) A/NK (molar ratio $Al_2O_3/(Na_2O + K_2O)$) versus A/CNK (molar ratio $Al_2O_3/(CaO + Na_2O + K_2O)$), and (d) K_2O versus Na_2O for the Early Cretaceous adakitic rocks and MMEs.

that partial melts from mafic granulites/amphibolites yield Na-rich melts (Petford and Gallagher, 2001; Rapp and Watson, 1995), while melting of TTG would normally have produced K-rich magmas (Zhang et al., 2017). The Early Cretaceous adakitic rocks in the MYRMB are characterized by high Na_2O/K_2O ratios from 1.1 to 2.7 (Table 1), which rules out the possibility of the TTG source. In terms of radiogenic isotopes, the $\varepsilon_{Nd}(t)$ and $(^{87}Sr/^{86}Sr)_i$ values of the adakitic rocks are distinguished from the Archean mafic granulites/amphibolites, but overlap with the coeval mafic rocks, revealing the existence of a juvenile mafic underplating lower crust as one of the magma sources. The lack of Archean model ages also indicates that contributions of ancient crustal materials, if any, were not evident in the mixing process (Table 2). The existence of the juvenile mafic lower crust was also identified in the giant Dexing porphyry Cu deposit area and played an important role in the formation of the ore-forming adakitic rocks in Dexing (Hou et al., 2013). Forasmuch as the adakitic rocks of Tongling in the north plot near the field of the lower continental crust (LCC) and those of Dexing in the south far away from the LCC field, input of ancient materials increases continuously with northward Nd—Sr isotope polarities (Fig. 8) and it is approximately parallel to coastward younging trend in the Jurassic–Cretaceous magmatism for the entire region, partially due to the subduction angle changed from shallow to steep subduction in that time interval (Li et al., 2013). With the highly varied trace element and Li–Nd–Sr isotopic compositions of the adakitic rocks taken into consideration, other than mixing of melts from two relatively homogeneous sources, alternatives such as melts from highly heterogeneous source of either the juvenile lower crust or the metasomatized sub-continental lithospheric mantle should not be omitted. The distinction between the mixing of magmas and mixing of sources is possible because partial melting greatly affects compatible/incompatible element ratios whereas ratios of incompatible elements will not be significantly affected (Supplemental File 3; Schiano et al., 2010). Therefore, mixing plots involving incompatible/incompatible element ratios show mixing relations for both two mixing scenarios, while a mixing trend in a plot with compatible/ incompatible element ratios strongly suggest mixing of magmas rather than mixing of sources. One approach to discriminate between these processes more effectively is to plot a $1/C^C–C^I/C^C$ diagram, where C is a compatible element (such as Cr, Ni, Co, and V), and I is incompatible element (e.g., Rb, Ba, Th, and U) with the condition $(D^I – 1) \approx -1$. Our data define a straight line with high $R^2 > 0.9$ in a 1/V–Rb/V discrimination diagram, thereby excluding partial melting (Supplemental File 3). Thus, the mixing processes shown in Supplemental File 3 must occur between magmas after their segregation from the solid source, rather than between their solid sources. Such a magma-mixing model is in full agreement with the ubiquitous MME occurrence as mafic magma blobs that became mixed with their host adakitic magma.

5.1.2. *Crustal contamination and fractional crystallization*

Since magmas must pass through the lower–middle crust before their emplacement, melt–rock interaction becomes the most likely way to generate the observed mixing relationships in the Early Cretaceous adakitic rocks from the MYRMB. Li et al. (2009) suggest that assimilation of crustal materials was not evident in the magmatic process due to lack of a correlation between SiO_2 and $\varepsilon_{Nd}(t)$ values of the adakitic rocks from the MYRMB. However, it should be noted that the processes of magma mixing and fractional crystallization both have an effect on the

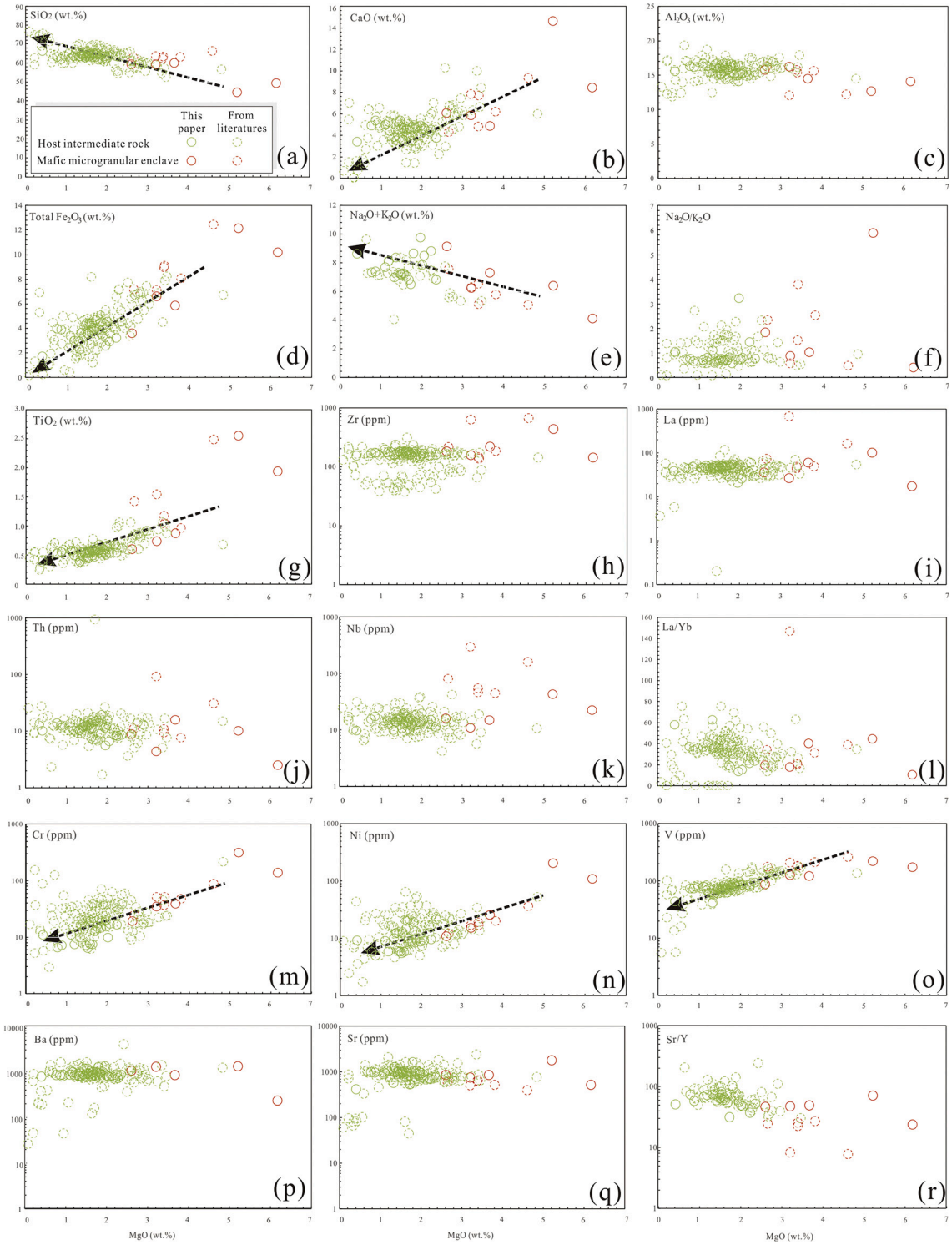

Fig. 5. Various oxide and trace element diagrams for the Early Cretaceous adakitic rocks and MMEs.

correlation, which thus was not conclusive. The xenocrystic zircons with $^{207}Pb/^{206}Pb$ ages of 2449–2522 Ma have been recognized in the adakitic rocks from the MYRMB, further confirming the contamination by upper crustal materials (Li et al., 2010). Although the majority of the Early Cretaceous adakitic rocks in the MYRMB plot into the mixing trend of the Cretaceous mafic rocks and EM II, the remaining plot along the trend to upper-middle continental crust (Fig. 8). This leads us to propose a possible scenario of the felsic crustal contamination during emplacement. The crustal contamination is verified by the Li isotopic data. The MMEs derived from the mantle source have low δ^7Li values and Li concentrations (Table 2), while the crustal melts from juvenile mafic underplating lower crust have high δ^7Li values and low Li concentrations, such as the typical I-type granite as melts from the mafic rocks (Fig. 11). Some adakitic rocks share high Li concentrations, indicating an input of high Li source, that is, the upper-middle continental crust like S-type granites with higher Li contents and lower δ^7Li values (Chen et al., 2018). To further determine the proportions of upper-middle continental crust materials in the process, we did δ^7Li–Li modeling

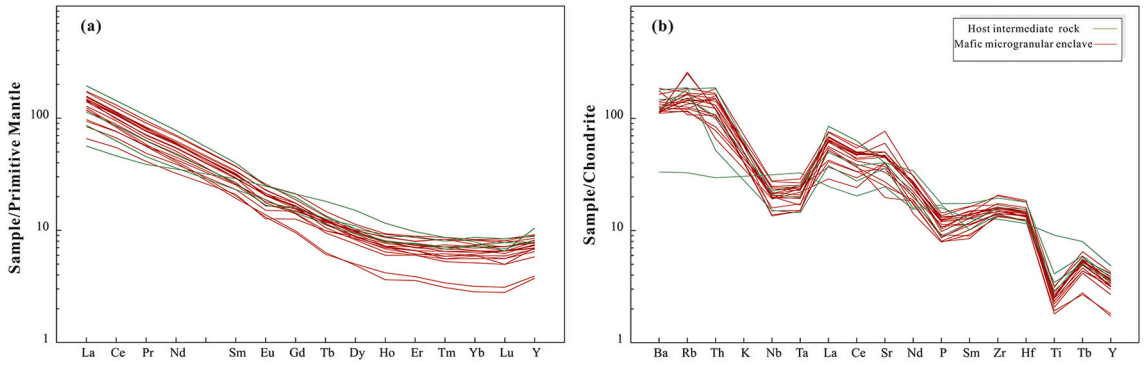

Fig. 6. Chondrite-normalized REE patterns (a) and primitive mantle-normalized spider diagrams (b) of the Early Cretaceous adakitic rocks and MMEs. Normalization values are from Sun and McDonough (1989).

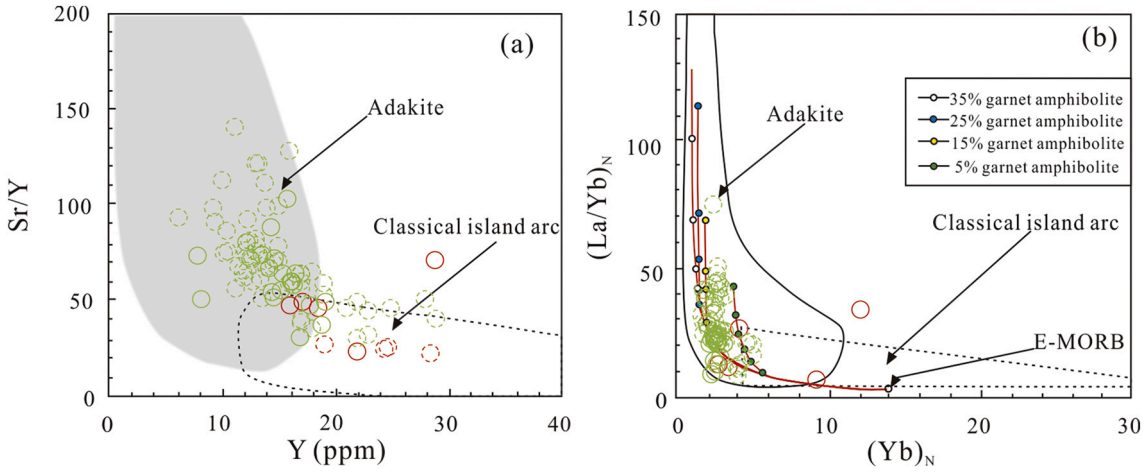

Fig. 7. (a) Sr/Y versus Y and (b) $(La/Yb)_N$ versus $(Yb)_N$ diagrams for the Early Cretaceous adakitic rocks and MMEs, discriminating between adakites and classical island arc of calc-alkaline compositions (Martin, 1999). Symbols as in Fig. 5.

based on a simple mixing model (Langmuir et al., 1978). The modeling suggests that incorporation of 1–10% upper-middle continental crustal materials can successfully explain the Li isotopic compositions and concentration of the adakitic rocks, assuming that the upper–middle continental crustal materials have Li = 150 ppm and $\delta^7Li = -2.75$, and that the most primitive melts from the mafic crust have Li = 7.83 ppm and $\delta^7Li = 10$ (Chen et al., 2018). Thus, although the mixing calculation shown in Fig. 11 is oversimplified, it strongly suggests that the Archean felsic continental crust material was another important source for the Early Cretaceous adakitic rocks in the MYRMB.

The Early Cretaceous adakitic rocks from the MYRMB show highly varied levels of MgO, $Mg^{\#}$, and compatible trace elements (Fig. 5m–o; Table 1), suggesting that they have undergone significant fractional crystallization. The positive correlation between Ni and Cr suggests that the parental magma might have undergone varying degrees of clinopyroxene or hornblende fractionation (Fig. 12a; Rollision, 1993). In addition, plagioclase fractionation is negligible based on the slightly negative or positive Eu anomalies in Fig. 6. The positive correlation between CaO and MgO and nearly constant Al_2O_3 concentrations also support the clinopyroxene fractionation, as abundant clinopyroxene would strongly alter the CaO/Al_2O_3 ratios (Fig. 5b and c). The hornblende and clinopyroxene fractionation can also be observed in the $(Yb)_N$ versus $(Ce/Yb)_N$ plot (Fig. 12b; Rollision, 1993).

5.2. Implications for adakite-like magma and related ore mineralization

The adakitic features, such as high Sr/Y ratios and low contents of HREEs (e.g., Y) in the Sr/Y versus Y diagrams (Fig. 7a), are probably caused by the following four factors. (i) Both the crustal and mantle sources of the adakitic rocks are characterized by high Sr/Y ratios and low Y contents, which will make these characteristics notable during partial melting processes (Fig. 6; Rollision, 1993). (ii) The H_2O-rich nature of the parental magma suppressed the early fractionation of plagioclase, as indicated by the abundance of euhedral hornblende in the Early Cretaceous adakitic rocks from the MYRMB (e.g., Tongshankou and Tongling areas; Chen et al., 2016; Chu et al., 2020). The subsequent fractionation of ferromagnesian phases, which could have contributed to the abundance of Sr and high Sr/Y ratios in the residual melts (a modeling in Fig. 7a; Chen et al., 2016) due to large Y partition coefficients for amphibole (Klein et al., 1997). (iii) The adakitic rocks may experience crustal contamination prior to emplacement. Crustal contaminants, such as greywacke, commonly show enrichment of LREEs and LILEs, and depletion of HREEs and depleted in high field strength elements (Rollision, 1993), which can elevate the Sr/Y and La/Yb ratios. (iv) MMEs within the host adakitic rocks evolved from the mafic magma via fractional crystallization and crustal contamination, which will elevate the Sr/Y and La/Yb ratios of the host as aforementioned. In summary, we contend that adakitic rocks are not necessarily formed under high-pressure conditions of crustal anatexis or within the garnet stability, which has usually been explained by an over-thickened crust or delamination of lower crustal rocks at mantle depths. Other factors, such as magma mixing and fractionation, may also play an important role in producing adakite-like features, which was used to be overlooked worldwide.

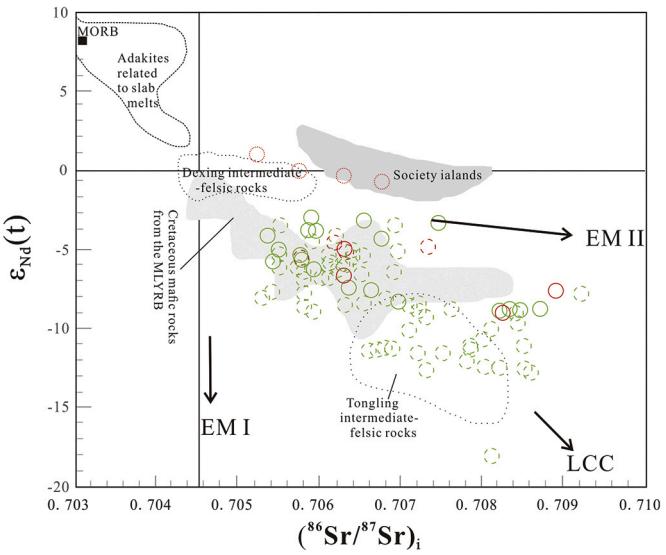

Fig. 8. Plots of $\varepsilon_{Nd}(t)$ versus $(^{87}Sr/^{86}Sr)_i$ for the Early Cretaceous adakitic rocks and MMEs. For comparison, also shown are data fields for the Cretaceous mafic rocks from the MYRMB (Xie et al., 2006; Wang et al., 2006), data fields for Tongling and Dexing intermediate-felsic rocks with adakitic signature (Hou et al., 2013; Wang et al., 2003), and data fields for Society islands (Hawkesworth et al., 1984). Symbols as in Fig. 5.

It is generally accepted that genesis of porphyry Cu–Mo–Au deposits are associated with high water content, sulfur-rich, and highly oxidized magmatic systems, with oxygen fugacities (fO_2) between the nickel–nickel oxide (NNO) or sulfide–sulfide oxide (SSO) and magnetite–hematite oxygen (MH) buffers (Ma et al., 2013; Mungall, 2002; Richards, 2011). As discussed before, the mantle source of the adakitic rocks in the MYRMB is EMII, suggesting an ancient metasomatized event (Table 2). The mantle-derived hydrous melts, subsequently evolving in the formation of the MMEs preserved in the host adakitic rocks, are characterized by abundance of euhedral hornblende and titanite in mineralogy, indicating a water-rich (≥4 wt%; Ridolfi et al., 2010) and high fO_2 (Foley and Wheller, 1990) signatures for their parental magma. The MMEs as well as the host adakitic rocks were formed under high fO_2 similar to highly oxidized I-type or magnetite-series granitoids (Rui et al., 1984), consistent with the low A/CNK values <1.1 (Fig. 4c) and Li concentrations and the high δ^7Li values (Fig. 11). In such a high oxidation state (higher than the SSO buffer, Mungall, 2002), sulfur would be dissolved in mantle-derived melts as oxidized forms. Chalcophile and siderophile elements within mantle sulfides are efficiently transported from the mantle source along with the melts (Hamlyn et al., 1985; Sillitoe, 1997). The hydrous magma as a mixture of enriched mantle melts and host felsic magmas may release a water-rich volatile phase to form a magmatic–hydrothermal ore-forming system (Burnham, 1997) during its ascent coupled with decreasing temperature and pressure, which is favorable to Cu—Au ore-forming. The existence of high temperature inclusions in the porphyry Cu–Mo–Au deposits in MYRMB indicates that these deposits were probably formed at high temperature and related to high temperature magmas (850–1150 °C) (Zhao et al., 2010). The main contribution of mantle-derived melts to the generation of the coeval Cu–Mo–Au deposits was heat, since the high temperature condition is favorable for the migration of Cu–Au–Fe ore-forming materials. The other end-member source of the adakitic rocks is the basaltic lower crustal rocks subjected to amphibolite-facies metamorphism during which the partition ratios of metals decrease remarkably

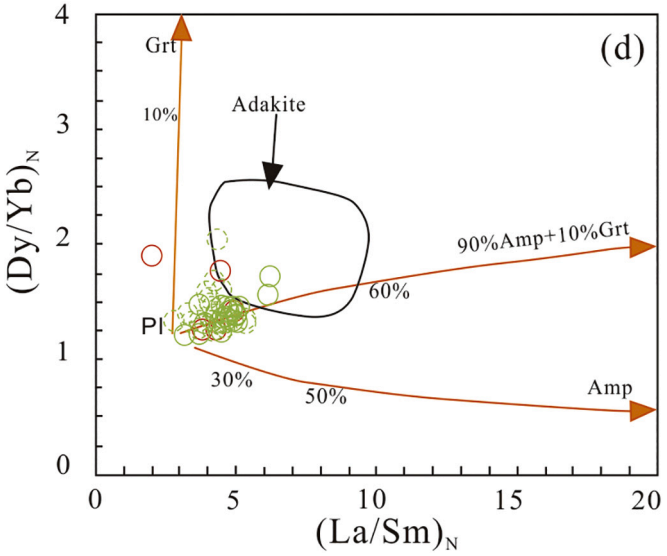

Fig. 10. $(La/Sm)_N$ versus $(Dy/Yb)_N$ diagram, showing Rayleigh fractional crystallization trends of garnet, amphibole, and 90% amphibole+10% garnet. The partition coefficients for amphibole and garnet are from Klein et al. (1997) and Ronov and Yaroshevsky (1976), respectively. Data source of adakites are from Xu et al. (2002) and Wang et al. (2006). Symbols as in Fig. 5.

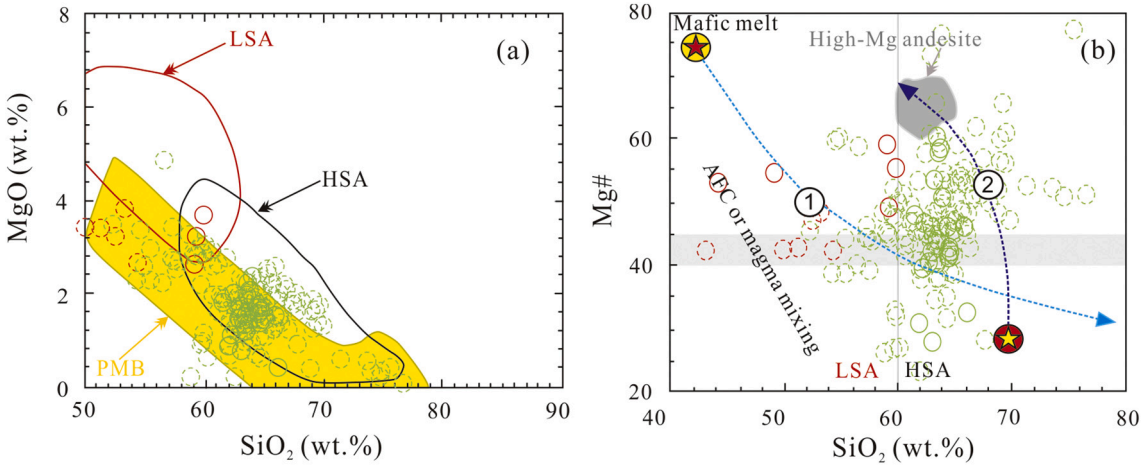

Fig. 9. (a) MgO versus SiO_2 diagram. PMB, experimental partial melts from basalts or amphibolites; LSA, low-silica adakite; HSA, high-silica adakite (modified after Martin et al. (2005)). (b) $Mg^{\#}$ value versus SiO_2 diagram. The fields of mantle-derived mafic melt and felsic melts from partial melting of garnet amphibolite and eclogite are from Kelemen (1995), Stern and Kilian (1996) and Rapp et al. (1999). Symbols as in Fig. 5.

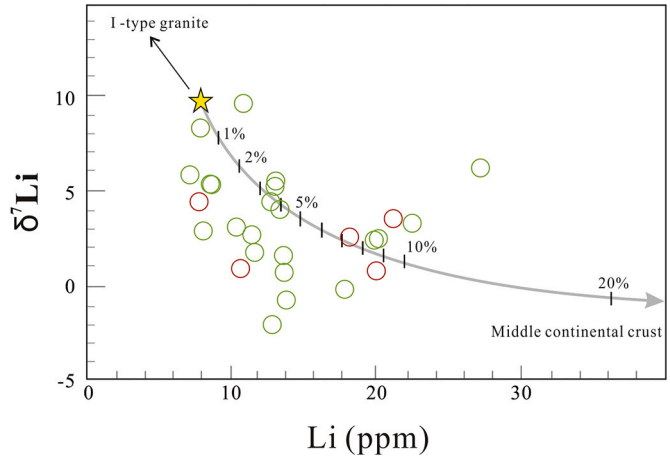

Fig. 11. Plot of Li versus δ^7Li of the Early Cretaceous adakitic rocks and MMEs. Symbols as in Fig. 5.

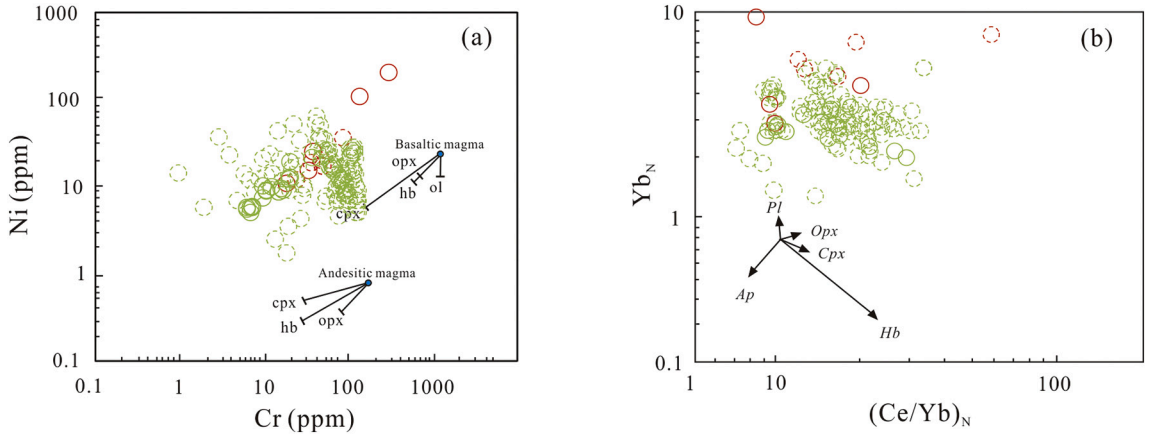

Fig. 12. Diagrams of crystal fractionation. (a) Ni versus Cr diagram. (b) Yb_N versus $(Ce/Yb)_N$ diagram. The partition coefficients are from Rollision (1993). Pl, plagioclase; Opx, orthopyroxene; Cpx, clinopyroxene; Hb, hornblende; Ap, apatite. Symbols as in Fig. 5.

(Khitarov et al., 1982; Urabe, 1987). This led the metals prone to exist in melt rather than vapor phase in high-pressure conditions. When the hybrid magma ascended to the middle-crust level, metals, such as Cu, in magma can be scavenged by exsolving magmatic fluid (Hedenduist and Lowenstern, 1994). During decompression, the adakitic rocks not only carry a lot of ore-forming materials, but also bring them from deep to shallow parts with ease, which agrees with the stable isotope (C, H, O, and S) data that ore-forming fluids were derived mainly from the mantle and subordinately from the crustal source (Zhou et al., 2015). Therefore, we consider that the hybrid magma (with high water content, high fO_2, and high sulfur) has the potential to form porphyry Mo—Cu deposits upon emplacement in the upper crust.

Therefore, we tentatively propose a model to explain the genesis and geodynamic setting of the Early Cretaceous adakitic rocks in the MYRMB. The late Mesozoic lithospheric extension caused asthenospheric mantle upwelling in the MYRMB, which may be created by oblique subduction of the Paleo-Pacific plate towards the Eurasia plate (Chu et al., 2020). *trans*-Lithospheric faults might be reactivated during the subduction, verified by the geophysical data of Moho along the MYRMB 3–4 km shallower than the vicinity (Zhai et al., 1992). The asthenospheric mantle upwelling provided additional heat to trigger the melting of lithosphere involving both an enriched lithospheric mantle peridotite and a juvenile underplating mafic lower crust. The partial melting of the enriched lithospheric mantle peridotite is preserved as the widespread Early Cretaceous mafic rocks and coeval MMEs within the host adakitic rocks in the MYRMB. The adakitic rocks are mixtures of the MMEs and the partial melts from the juvenile underplating mafic lower crust, which experienced significant fractional crystallization and minor crustal contamination during magma evolution. The salient geochemical features of the adakitic rocks, such as elevated La/Yb and Sr/Y, might be affected by complex petrogenetic processes, i.e., nature of the sources, fractional crystallization, crustal contamination, or magma mixing, rather than controlled by the P–T conditions of crustal anatexis alone as previously thoughts (Martin et al., 2005), which might have also been usually overlooked in the research of adakitic rocks. The adakitic rocks harbor a key to calibrating important crust–mantle interaction, monitoring critical geodynamic process as well as probing essential ore-forming mechanism scenario.

6. Conclusions

The salient conclusions arising from our synthesis have been reached:

Field and petrological observations, and whole-rock chemical data all point to the formation of the Early Cretaceous adakitic rocks in the Edong district through magma mixing between felsic melts from a juvenile lower crust and mafic melts from an enriched mantle source, fractional crystallization and crustal contamination. High water content,

and high oxygen and sulfur fugacity of hybrid magma are favorable for the polymetallic mineralization in MYRMB, which also recorded the Early Cretaceous crust–mantle interaction during the subduction of the Paleo-Pacific plate.

Declaration of Competing Interest

We declare that we have no financial and personal relationships with other people or organizations that can in appropriately influence our work, there is no professional or other personal interest of any nature or kind in any product, service and/or company that could be constructed as influencing the position presented in or the review of, the manuscript entitled.

Acknowledgements

Comments and suggestions from two anonymous reviewers and the Editor-in-Chief Greg Shellnutt improved the paper greatly. We acknowledge the financial support from the Science Foundation of China University of Petroleum, Beijing (No. 2462017YJRC032 and 2462021YXZZ004), the National Natural Science Foundation of China (No. 42002238 and 41804045), Opening Foundation of Key Laboratory of Mineral Resources Evaluation in Northeast Asia, Ministry of Land and Resources (No. DBY-KF-19-03), and Opening Foundation of Key Laboratory of Regional Geology and Mineralization, Hebei GEO University.

Appendix A. Supplementary data

Supplementary data to this article can be found online at https://doi.org/10.1016/j.lithos.2021.106308.

References

Burnham, C.W., 1997. Magmas and hydrothermal fluids. In: Barnes, H.L. (Ed.), Geochemistry of Hydrothermal Ore Deposits, 3rd Edition. John Wiley and Sons, New York, pp. 63–123.
Chen, B., Chen, Z.C., Jahn, B.M., 2009. Origin of mafic enclaves from the Taihang Mesozoic orogen, north China craton. Lithos 110, 343–358.
Chen, B., Gu, H.O., Chen, Y.J., Sun, K.K., Chen, W., 2018. Lithium isotope behaviour during partial melting of metapelites from the Jiangnan Orogen, South China: implications for the origin of REE tetrad effect of F-rich granite and associated rare-metal mineralization. Chem. Geol. 483, 372–384.
Chen, C.J., Chen, B., Li, Z., Wang, Z.Q., 2016. Important role of magma mixing in generating the Mesozoic monzodioritic–granodioritic intrusions related to Cu mineralization, Tongling, East China: evidence from petrological and in situ Sr–Hf isotopic data. Lithos 248–251, 80–93.
Chen, J.F., Yan, J., Xie, Z., Xu, X., Xing, F., 2001. Nd and Sr isotopic compositions of igneous rocks from the lower Yangtze region in eastern China: constraints on sources. Phys. Chem. Earth Solid Earth Geod. 26, 719–731.
Chu, G.B., Chen, H.Y., Falloon, T.J., Han, J.S., Zhang, S.T., Cheng, J.M., Zhang, X.B., 2020. Early cretaceous mantle upwelling and melting of juvenile lower crust in the Middle–lower Yangtze River Metallogenic Belt: example from Tongshankou Cu–(Mo–W) ore deposit. Gondwana Res. 83, 183–200.
Clynne, M.A., 1999. A complex magma mixing origin of rock erupted in 1915, Lassen Peak, California. J. Petrol. 40, 105–132.
Defant, M.J., Richerson, M., De Boer, J.Z., Strwart, R.H., Maury, R.C., Bellon, H., Drummond, M.S., 1991. Dacite genesis via both slab melting and differentiation: petrogenesis of La Yeguada volcanic complex, Panama. J. Petrol. 32, 1101–1142.
Defant, M.J., Jackson, T.E., Drummond, M.S., De Boer, J.Z., Bellon, H., Feigenson, M.D., Maury, R.C., Stewart, R.H., 1992. Adakites from Panama and Costa Rica. J. Geol. Soc. 149, 569–579.
Drummond, M.S., Defant, M.J., 1990. A model from trondhjemite–tonalite–dacite genesis and crustal growth via slab-derived: Archaean to modern comparisons. J. Geophys. Res. 95, 21503–21521.
Evans, O.C., Hanson, G.N., 1997. Late- to post kinematic Archean granitoids of the S.W. Superior Province: Derivation through direct mantle melting. In: de Wit, M.J., Ashwal, L.D. (Eds.), Greenstone Belts: Oxford. Oxford University Press, UK, pp. 280–295.
Feeley, T.C., Wilson, L.F., Underwood, S.J., 2008. Distribution and compositions of magmatic inclusions in the Mount Helen dome, Lassen Volcanic Center, California: insights into magma chamber processes. Lithos 106, 173–189.
Foley, S.F., Wheller, G.E., 1990. Parallels in the origin of the geochemical signatures of island arc volcanics and continental potassic igneous rocks: the role of residual titanites. Chem. Geol. 85, 1–18.
Frey, F.A., Prinz, M., 1978. Ultramafic inclusions from San Carlos, Arizona: petrologic and geochemical data bearing on their petrogenesis. Earth Planet. Sci. Lett. 38, 129–176.
Gao, S., Yang, J., Zhou, L., Li, M., Hu, Z.C., Guo, J.L., Yuan, H.L., Gong, H.J., Xiao, G.Q., Wei, J.Q., 2011. Age and growth of the Archean Kongling Terrain, South China, with emphasis on 3.3 Ga granitoid gneisses. Am. J. Sci. 311, 153–182.
Griffin, W.L., Wang, X., Jackson, S.E., Pearson, N.J., O'Reilly, S.Y., 2002. Zircon geochemistry and magma mixing, SE China: in-situ analysis of Hf isotopes, Tonglu and Pingtan igneous complexes. Lithos 61, 237–269.
Hamlyn, P.R., Keays, R.R., Cameron, W.E., Crawford, A.J., Waldron, H.M., 1985. Precious metals in magnesian low-Ti lavas: implications for metallogenesis and sulfur saturation in primary magmas. Geochim. Cosmochim. Acta 49, 1797–1811.
Hawkesworth, C.J., Rogers, N.W., van Calsteren, P.W.C., Menzies, M.A., 1984. Mantle enrichment processes. Nature 311, 331–335.
Hedenduist, J.W., Lowenstern, J.B., 1994. The role of magmas in the formation of hydrothermal ore deposits. Nature 370, 519–527.
Hofmann, A.W., 1988. Chemical differentiation of the Earth: the relationship between mantle, continental crust, and oceanic crust. Earth Planet. Sci. Lett. 90, 297–314.
Hofmann, A.W., 1997. Mantle geochemistry: the message from oceanic volcanism. Nature 385, 219–229.
Holden, P., Halliday, A.N., Stephens, W.E., 1987. Neodymium and strontium isotope content of microdiorite enclaves points to mantle input to granitoid production. Nature 330, 53–56.
Hou, Z.Q., Pan, X.F., Li, Q.Y., Yang, Z.M., Song, Y.C., 2013. The giant Dexing porphyry Cu–Mo–Au deposit in east China: product of melting of juvenile lower crust in an intracontinental setting. Mineral. Deposita 48, 1019–1045.
Irvine, T.H., Baragar, W.R.A., 1971. A guide to the chemical classification of the common volcanic rocks. Can. J. Earth Sci. 8, 523–548.
Jahn, B.M., Wu, F.Y., Lo, C.H., Tsai, C.H., 1999. Crust–mantle interaction induced by deep subduction of the continental crust: geochemical and Sr–Nd isotopic evidence from post-collisional mafic–ultramafic intrusions of the northern Dabie complex, central China. Chem. Geol. 157, 119–146.
Kelemen, P.B., 1995. Genesis of high Mg# andesites and the continental crust. Contrib. Mineral. Petrol. 120, 1–19.
Kelemen, P.B., Hanghøj, K., Greene, A.R., 2003. One view of the geochemistry of subduction-related magmatic arcs, with an emphasis on primitive andesite and lower crust. Treat. Geochem. 3, 593–659.
Kemp, A.I.S., 2004. Petrology of high-Mg, low-Ti igneous rocks of the Glenelg River complex (SE Australia) and the nature of their interaction with crustal melts. Lithos 78, 119–156.
Kemp, A.I.S., Hawkesworth, C.J., 2006. Using hafnium and oxygen isotopes in zircons to unravel the record of crustal evolution. Chem. Geol. 226, 144–162.
Khitarov, N.I., Malinin, S.P., Lebedev, Y.B., 1982. The distribution of Zn, Cu, Pb, Mo between a fluid phase and a silicate melt of granitic composition at high temperatures and pressures. Geochem. Int. 19, 123–136.
Klein, M., Stosch, H.G., Seck, H.A., 1997. Partitioning of high field-strength and rare-earth elements between amphibole and quartz-dioritic to tonalitic melts: an experimental study. Chem. Geol. 138, 257–271.
Langmuir, C.H., Vocke, R.D., Hanson, G.N., Hart, S.R., 1978. A general mixing equation with applications to Icelandic basalts. Earth Planet. Sci. Lett. 37, 380–392.
Li, J.W., Zhao, X.F., Zhou, M.F., Vasconcelos, P., Ma, C.Q., Deng, X.D., de Souza, Z.S., Zhao, Y.X., Wu, G., 2008. Origin of the Tongshankou porphyry-skarn Cu–Mo deposit, eastern Yangtze craton, Eastern China: geochronological, geochemical, and Sr–Nd–Hf isotopic constraints. Mineral. Deposita 43, 315–336.
Li, J.W., Zhao, X.F., Zhou, M.F., Ma, C.Q., de Souza, Z.S., Vasconcelos, P., 2009. Late Mesozoic magmatism from the Daye region, eastern China: U–Pb ages, petrogenesis, and geodynamic implications. Contrib. Mineral. Petrol. 157, 383–409.
Li, X.H., McCulloch, M.T., 1996. Secular variation on the Nd isotopic composition of Neoproterozoic sediments from the southern margin of the Yangtze block: evidence for a Proterozoic continental collision in southeast China. Precambrian Res. 76, 67–76.
Li, X.H., Li, W.X., Wang, X.C., Li, Q.L., Liu, Y., Tang, G.Q., Gao, Y.Y., Wu, F.Y., 2010. SIMS U–Pb zircon geochronology of porphyry Cu–Au–(Mo) deposits in the Yangtze River Metallogenic Belt, eastern China: magmatic response to early cretaceous lithospheric extension. Lithos 119, 427–438.
Li, X.H., Li, Z.X., Li, W.X., Wang, X.C., Gao, Y., 2013. Revisiting the "C-type adakites" of the lower Yangtze River Belt, central eastern China: in-situ zircon Hf-O isotope and geochemical constraints. Chem. Geol. 345, 1–15.
Ling, M.X., Wang, F.Y., Ding, X., Hu, Y.H., Zhou, J.B., Zartman, R.E., Yang, X.Y., Sun, W. D., 2009. Cretaceous ridge subduction along the lower Yangtze River belt, eastern China. Econ. Geol. 104, 303–321.
Ma, X.H., Chen, B., Yang, M.C., 2013. Magma mixing origin for the Aolunhua porphyry related to Mo–Cu mineralization, eastern Central Asian Orogenic Belt. Gondwana Res. 24, 1152–1171.
Mao, J.W., Wang, Y.T., Lehmann, B., Yu, J.J., Du, A.D., Mei, Y.X., Li, Y.F., Zang, W.S., Stein, H.J., Zhou, T.F., 2006. Molybdenite Re–Os and albite $^{40}Ar/^{39}Ar$ dating of Cu–Au–Mo and magnetite porphyry systems in the Yangtze River valley and metallogenic implications. Ore Geol. Rev. 29, 307–324.
Mao, J.W., Xie, G.Q., Duan, C., Pirajno, F., Ishiyama, D., Chen, Y.C., 2011. A tectono-genetic model for porphyry-skarn-stratabound Cu–Au–Mo–Fe and magnetite- apatite deposits along the Middle–lower Yangtze River Valley, Eastern China. Ore Geol. Rev. 43, 293–314.
Martin, H., 1999. Adakitic magmas: modern analogues of Archaean granitoids. Lithos 46, 411–429.

Martin, H., Smithies, R.H., Rapp, R., Moyen, J.F., Champion, D., 2005. An overview of adakite, tonalite–trondhjemite–granodiorite (TTG), and sanukitoid: Relationships and some implications for crustal evolution. Lithos 79, 1–24.
Middlemost, E.A., 1994. Naming materials in the magma/igneous rock system. Earth Sci. Rev. 37, 215–224.
Mungall, J.E., 2002. Roasting the mantle: slab melting and the genesis of major Au and Au-rich Cu deposits. Geology 30, 915–918.
Noyes, H., Frey, F.A., Wones, D.R., 1983. A tale of two plutons: geochemical evidence bearing on the origin and differentiation of the Red Lake and Eagle Peak plutons, central Sierra Nevada, California. J. Geol. 91, 487–509.
Oyarzún, R., Márquez, A., Lillo, J., López, I., Rivera, S., 2001. Giant versus small porphyry copper deposits of cenozoic age in northern Chile: adakitic versus normal calc-alkaline magmatism. Mineral. Deposita 36, 794–798.
Pan, Y.M., Dong, P., 1999. The lower Yangtze (Yangtze/Changjiang) metallogenic belt, east central China: intrusion- and wall rock-hosted Cu–Fe–Au, Mo, Zn, Pb, Ag deposits. Ore Geol. Rev. 15, 177–242.
Petford, N., Gallagher, K., 2001. Partial melting mafic (amphibolitic) lower crust by periodic influx of basaltic magma. Earth Planet. Sci. Lett. 193, 483–499.
Qian, Q., Hermann, J., 2013. Partial melting of lower crust at 10–15 kbar: constraints on adakite and TTG formation. Contrib. Mineral. Petrol. 165 (6), 1195–1224.
Rapp, R.P., Watson, E.B., 1995. Dehydration melting of metabasalt at 8–32 kbar: implications for continental growth and crust-mantle recycling. J. Petrol. 36, 891–931.
Rapp, B.R., Shimizu, N., Norman, M.D., Applegate, G.S., 1999. Reaction between slab derived melts and peridotite in the mantle wedge: experimental constraints at 3.8 GPa. Chem. Geol. 160, 335–356.
Rapp, R.P., Shimizu, N., Norman, M.D., 2003. Growth of early continental crust by partial melting of eclogite. Nature 425, 605–609.
Ridolfi, F., Renzulli, A., Puerini, M., 2010. Stability and chemical equilibrium of amphibole in calc-alkaline magmas: an overview, new thermobarometric formulations and application to subduction-related volcanoes. Contrib. Mineral. Petrol. 160, 45–66.
Rollision, H.R., 1993. Using Geochemical Data: Evaluation, Presentation, Interpretation. Longma Singapore Publishers (Pte) Ltd., Singapore.
Ronov, A.B., Yaroshevsky, A.A., 1976. A new model for the chemical structure of the Earth's crust. Geokhimiya 13, 89–121.
Rui, Z.Y., Huang, C.K., Qi, G.M., Xu, J., Zhang, H.T., 1984. Porphyry Copper (Molybdenum) Deposits of China. Geological Publishing House, Beijing, p. 350 (in Chinese with English abstr.).
Sajona, F.G., Maury, R.C., 1998. Association of adakites with gold and copper mineralization in the Philippines. Compt. Rendus Geosci. 326, 27–34.
Schiano, P., Monzier, M., Eissen, J.P., Martin, H., Koga, K.T., 2010. Simple mixing as the major control of the evolution of volcanic suites in the Ecuadorian Andes. Contrib. Mineral. Petrol. 160, 297–312.
Schmidt, M.W., Dardon, A., Chazot, G., Vannucci, R., 2004. The dependence of Nb and Ta rutile-melt partitioning on melt composition and Nb/Ta fractionation during subduction processes. Earth Planet. Sci. Lett. 226, 415–432.
Sillitoe, R.H., 1997. Characteristic and controls of the largest porphyry copper–gold and epithermal gold deposits in the circum-Pacific region. Aust. J. Earth Sci. 44, 373–388.
Smithies, R.H., Champion, D.C., 2000. The Archaean high-Mg diorite suite: Links to tonalite–trondhjemite–granodiorite magmatism and implications for early Archaean crustal growth. J. Petrol. 41, 1653–1671.
Stern, C.R., Kilian, R., 1996. Role of the subducted slab, mantle wedge and continental crust in the generation of adakites from the Austral Volcanic Zone. Contrib. Mineral. Petrol. 123, 263–281.
Sun, S.S., McDonough, W.F., 1989. Chemical and isotopic systematics of oceanic basalts: implications for mantle composition and processes. Geological Society Special Pubication, London 42, 313–345.
Tasumi, Y., Hamilton, D.L., Nesbitt, R.W., 1986. Chemical characteristics of fluid phase released from a subducted lithosphere and the origin of arc magmas: evidence from high pressure experiments and natural rocks. J. Volcanol. Geotherm. Res. 29, 293–309.
Urabe, T., 1987. The effect of pressure on the partioning ratios of lead and zinc between vapor and rhyolite melts. Econ. Geol. 82, 1049–1052.
Wan, Y.S., Li, R.W., Wilde, S.A., Liu, D.Y., Chen, Z.Y., Yan, L., Song, T.R., Yin, X.Y., 2005. UHP metamorphism and exhumation of the Dabie Orogen, China: evidence from SHRIMP dating of zircon and monazite from a UHP granitic gneiss cobble from the Hefei Basin. Geochim. Cosmochim. Acta 69, 4333–4348.
Wang, Q., Zhao, Z.H., Xu, J.F., Li, X.H., Bao, Z.W., Xiong, X.L., Liu, Y.M., 2003. Petrogenesis and metallogenesis of the Yanshanian adakite-like rocks in the Eastern Yangtze Block. Sci. China Ser. D Earth Sci. 46, 164–176.
Wang, Q., Zhao, Z.H., Bao, Z.W., Xu, J.F., Liu, W., Li, C.F., Bai, Z.H., Xiong, X.L., 2004. Geochemistry and petrogenesis of the Tongshankou and Yinzu adakitic intrusive rocks and the associated porphyry copper–molybdenum mineralization in southeast Hubei, east China. Resour. Geol. 54, 137–152.
Wang, Q., Wyman, D.A., Xu, J.F., Zhao, Z.H., Jian, P., Xiong, X.L., Bao, Z.W., Li, C.F., Bai, Z.H., 2006. Petrogenesis of cretaceous adakitic and shoshonitic igneous rocks in the Luzong area, Anhui Province (eastern China): implications for geodynamics and Cu–Au mineralization. Lithos 89, 424–446.
White, A.J.R., Chappell, B.W., Wyborn, D., 1999. Application of the restite model to the Deddick granodiorite and its enclaves–a reinterpretation of the observations and data of Maas et al. (1997). J. Petrol. 40, 413–421.
Wilson, W., 1989. Igneous Petrogenesis. Unwin Hyman, London, pp. 327–373.
Xiao, L., Clemens, J.D., 2007. Origin of potassic (C-type) adakite magmas: experimental and field constraints. Lithos 95, 399–414.
Xie, G.Q., Mao, J.W., Li, R., Zhou, S.D., Ye, H.R., Yan, Q.R., Zhang, Z.S., 2006. SHRIMP U–Pb age of the Dasi Formation volcanic rocks from southeastern Hubei, mid–lower reaches of the Yangtze River. Sci. China Ser. D Earth Sci. 51, 2283–2291.
Xie, G.Q., Mao, J.W., Li, R.L., Beirlein, F.P., 2008. Geochemistry and Nd–Sr isotopic studies of late Mesozoic granitoids in the southeastern Hubei province, Middle–lower Yangtze River belt, Eastern China: petrogenesis and tectonic setting. Lithos 104, 216–230.
Xie, G.Q., Mao, J.W., Zhao, H.J., 2011. Zircon U–Pb geochronological and Hf isotopic constraints on petrogenesis of late Mesozoic intrusions in the Southeast Hubei Province, Middle–lower Yangtze River belt (MLYRB), East China. Lithos 125, 693–710.
Xu, J.F., Shinjo, R., Defant, M.J., Wang, Q., Rapp, R.P., 2002. Origin of Mesozoic adakitic intrusive rocks in the Ningzhen area of East China: partial melting of delaminated lower continental crust? Geology 30, 1111–1114.
Zhai, Y.S., Yao, S.Z., Lin, X.D., Zhou, X.N., Wan, T.F., Jin, F.Q., Zhou, Z.G., 1992. Fe–Cu–(Au) Metallogeny of the Middle–Lower Changjiang Region. Geological Publishing House, Beijing (235 pp., in Chinese).
Zhai, Y.S., Xiong, Y.L., Yao, S.Z., Lin, X.D., 1996. Metallogeny of copper and iron deposits in the Eastern Yangtse Craton, east-central China. Ore Geol. Rev. 11, 229–248.
Zhang, S.W., Wei, C.J., Duan, Z.Z., 2017. Petrogenetic simulation of the Archean trondhjemite from Eastern Hebei, China. Sci. China Earth Sci. 60, 958–971.
Zhao, G.C., Cawood, P.A., 2012. Precambrian geology of China. Precambrian Res. 222–223, 13–54.
Zhao, H.J., Mao, J.W., Xiang, J.F., Zhou, Z.H., Wei, K.T., Ke, Y.F., 2010. Mineralogy and Sr–Nd–Pb isotopic compositions of quartz diorite from the Tonglushan deposit, Hubei Province. Acta Petrol. Sin. 26, 768–784 (in Chinese with English abstract).
Zhou, T.F., Fan, Y., Yuan, F., Lu, S.M., Shang, S.G., David, C., Sebastien, M., Zhao, G.C., 2008. Geochronology of the volcanic rocks in the Lu–Zong basin and its significance. Sci. China Ser. D Earth Sci. 51, 1470–1482.
Zhou, T.F., Wang, S.W., Fan, Y., Yuan, F., Zhang, D.Y., White, N.C., 2015. A review of the intracontinental porphyry deposits in the Middle–lower Yangtze River Valley metallogenic belt, Eastern China. Ore Geol. Rev. 65, 433–456.